Condensin positioning at telomeres by Taz1 promotes telomere disjunction in anaphase

Léonard Colin [2, 3 †], Céline Reyes[1†], Julien Berthezene[1], Laetitia Maestroni [5], Laurent Modolo [2,3], Esther Toselli [2,3], Nicolas Chanard [1,4], Stephane Schaak[1,4], Olivier Cuvier [1,4], Yannick Gachet [1]*, Stéphane Coulon* [5], Pascal Bernard [2, 3]*, Sylvie Tournier [1]*

[1] MCD, Centre de Biologie Intégrative, Université de Toulouse, CNRS, UPS, 31062 Toulouse Cedex, France"

[2] CNRS - Laboratory of Biology and Modelling of the Cell, UMR 5239, Lyon, France

[3] ENS de Lyon, Univ. Lyon, 46 allée d'Italie, site Jacques Monod, F-69007, Lyon, France

[4] CBI, MCD-UMR5077, CNRS, Chromatin dynamics team, 31062, Toulouse

[5] CNRS, INSERM, Aix Marseille Univ, Institut Paoli-Calmettes, CRCM, Equipe labellisée par la Ligue Nationale contre le Cancer, Marseille, F-13009, France

* Co-corresponding authors: Sylvie Tournier sylvie.tournier-gachet@univ-tlse3.fr , Pascal Bernard pascal.bernard@ens-lyon.fr , Stéphane Coulon stephane.coulon@inserm.fr and Yannick Gachet yannick.gachet@univ-tlse3.fr

[†] These authors participate equally to this work.

The localization of condensin along chromosome arms is crucial for chromosome segregation in anaphase. Condensin is also enriched at telomeres but how and for what function remains elusive. Here we show that Taz1, the main component of the Shelterin complex that ensures telomeric functions, acts as a positioning device to enrich condensin at telomeres in fission yeast. High condensin occupancy at telomeres is needed for their full disjunction in anaphase. Consistent with a cis-acting process, condensin drives telomere separation independently of the decatenation activity of Topoisomerase II also required for chromosome arm separation. Our results reveal a cis-acting pathway that enriches condensin at telomeres to promote their separation during mitosis.

One-Sentence Summary: The telomeric protein Taz1 promotes the accumulation of condensin at telomeres that drives their disjunction in anaphase.

In eukaryotes, chromosome segregation relies on the migration of sister-centromeres towards the opposite poles of the mitotic spindle and on the stiffness of chromosome arms conferred by condensin, which transmits traction forces from centromere to telomeres. Condensin is a five-subunit DNA-translocase of the SMC family (*1–3*). Current data indicate that the holocomplex shapes mitotic chromosomes by forming loops of chromatin (*2*, *4*, *5*). Condensin also promotes the removal of interlinks between sister-chromatids by directing the activity of Topoisomerase II (Top2) towards decatenation (*6–8*). We and others previously showed that the separation of sister-telomeres in anaphase involves condensin regulators such as Cdc14 phosphatase in budding yeast (*9*), and Aurora-B kinase in fission yeast (*10*, *11*). Condensin is enriched at telomeres from yeasts to mammals (*12*, *13*), but whether it plays any role in their separation remain unknown. Telomeres contain repetitive sequences bound and protected by the shelterin protein complex (*14*). Although the human shelterin protein TRF1 had been reported to bind the kleisin subunit of condensin II (*15*), no conclusive evidence for the localization and possible function of condensin at telomeres was provided.

In a wide range of species, condensin displays a broad and basal distribution along the genome, punctuated by peaks of high occupancy at centromeres, telomeres, rDNA repeats, and in the vicinity of highly expressed genes (*12*). To revisit the localization of condensin at telomeres in fission yeast, we generated calibrated ChIP-sequencing (ChIP-seq) maps of its kleisin subunit Cnd2 tagged with GFP (Cnd2-GFP) from metaphase-arrests. The *cut3-477* mutation in the $Cut3^{SMC4}$ ATPase of condensin, which reduces its binding genome-wide (Fig. S1), controlled for the localization of the holocomplex. ChIP-seq reads were mapped on a fission yeast genome that contains a full-length subtelomere and telomere repeats at the right end of chromosome 2 (TEL2R, Fig1.A) and read-counts were corrected for biases caused by telomere repeats (supplementary text and Fig. S2-S3). In wild-type, Cnd2-GFP was clearly enriched at telomere repeats and over the

adjacent STE1 element (Fig. 1B), while a basal level of association was observed at more distal elements (Fig. S4A). Importantly, Cnd2-GFP occupancy at TEL2R was reduced in a *cut3-477* background (Fig. 1B and S4A). Thus, these results suggest that fission yeast condensin is enriched at telomeres in metaphase.

Fission yeast shelterin is composed of Taz1 (a DNA-binding protein homologous to human TRF1-2), Rap1, Poz1, Tpz1, Pot1 and Ccq1. Using calibrated ChIP-qPCR, we found that Cnd2-GFP occupancy was reduced at TEL2R in *taz1*Δ cells, while remaining unchanged at the kinetochore and within chromosome arms (Fig. 1C). In contrast, the *rap1*Δ mutant showed no change compared to wild-type. A different internal calibration produced similar results (Fig. S4B). It is unlikely for telomere length to titrate Cnd2-GFP away from TEL2R since *rap1*Δ and *taz1*Δ mutants show a similar increase in telomere length *(16)*. Taz1 also binds discrete sites within chromosome arms (*17*), but the level of Cnd2-GFP was basal at non-telomeric Taz1 islands (Fig. 1D and S5), arguing that Taz1 increases condensin occupancy specifically in a telomeric context. We observed no physical interaction between condensin and Taz1, either by co-immunoprecipitation or by yeast two-hybrid assay (our unpublished data), suggesting that Taz1 does not directly recruit condensin. Thus, Taz1 acts as a cis-acting positioning factor for condensin at telomeres.

Next, we impaired condensin in mitotic cells expressing fluorescently tagged Taz1 (Taz1-GFP) to assess telomere behavior and Cdc11 (Cdc11-CFP) to follow progression through anaphase via spindle pole bodies (SPBs) (Fig. 2A). Having three chromosomes, cells with more than six Taz1-GFP foci indicates telomeres separation and 12 foci full sister-telomeres separation (*10*). At the restrictive temperature, thermosensitive condensin mutant cells *cut3-477, cut14-90* or *cut14-208* rarely displayed more than six telomeric dots during anaphase (Fig. 2A and S6A-B; Movie S1), even when centromeres were segregated at the opposite poles. Thus, condensin is required for

telomeres disjunction in anaphase. To assess whether persistent entanglements underpin telomeres non-disjunction, we examined cold sensitive *top2-250* mutant cells whose Top2-decatenation activity drops below detection at 20°C *in vitro* (*18*). Consistent with a loss of decatenation, *top2-250* cells exhibited chromatin bridges and lagging centromeres (Fig. S6C-D). Yet, telomere disjunction remained effective, even within chromatin bridges (Fig. 2B-C). Top2 decatenation activity is therefore dispensable for telomere separation during anaphase. The corollary is that condensin-driven telomere separation is largely independent of DNA-decatenation by Top2.

To assess whether condensin shapes telomeres organization prior to anaphase, we generated Hi-C maps in metaphase (Fig. 3 and S7). As reported (*19*), we observed centromere-to-centromere and telomere-to-telomere contacts between chromosomes in wild-type cells (Fig. 3B and S7B). In the *cut14-208* condensin mutant, contact frequencies within chromosome arms were reduced, revealing in the differential map Topologically-Associated Domains (TADs) formed by condensin (*19*) up to subtelomeres. Strikingly, inter- and intra- chromosomal contacts were increased at telomeres but not at centromeres in the condensin mutant (Fig. 3C-D and S7C-D). Aggregating Hi-C signals at chromosome ends further revealed that intra-chromosomal contacts dominate over inter-chromosomal contacts in wild-type and mutant cells (Fig. 3E and S7E). These data suggest that fission yeast chromosomes conserve their Rabl configuration (*20*) upon mitotic entry, with telomeres clustered together, and that condensin drives their declustering into pairs of sister-telomeres as cells progress towards metaphase (Fig. 3 and S7), possibly by folding chromosome arms, and their full-separation in anaphase (Fig. 2).

Telomere separation during anaphase is impaired in *taz1*Δ cells grown at low temperature (*21*), suggesting a causal relationship with reduced condensin occupancy at telomeres (Fig. 1). In line with this, the *taz1*Δ and *cut3-477* mutations exhibited a negative genetic interaction at 32°C

and 34°C (Fig. 4A). Analyzing telomere separation in single and double mutant cells by counting the number of fluorescent Ccq1-GFP foci (Fig. 4B) confirmed the impaired separation of telomeres in *cut3-477* cells at 32°C (Fig. 4B and S8) and importantly, revealed a synergistic increase of telomere non-disjunctions in the *cut3-477 taz1*Δ double mutant at 32°C (Fig. 4C). In addition, we observed reproducible changes in telomere length in thermosensitive condensin mutants propagated at the semi-permissive temperature (Fig. S9), consistent with an accumulation of telomeric stress throughout anaphases. Altogether, these data substantiate the idea that condensin enrichment at telomeres, set-up by Taz1, is a limiting parameter for their disjunction during anaphase and for their structural stability.

Here we show that the enrichment of fission yeast condensin at telomeres results from a cis-acting pathway that involves Taz1^{TRF1-2} protein, that condensin activity is needed for the separation of telomeres, and that combining the lack of Taz1 with condensin deficiency synergistically impair telomere disjunction. Importantly, we also show that condensin-oriented decatenation by Top2 is dispensable for telomere disjunction, implying that separating chromosome arms is not the mere driver of telomere disjunction in anaphase. We therefore propose that Taz1-dependent enrichment of condensin at telomeres drives telomere separation. Given the presence of condensin-dependent TADs at subtelomeres, it is tempting to speculate that condensin-mediated loop extrusion (*2*, *3*) provides the power stroke to disentangle telomeres, even when Top2 is impaired thanks to the proximity of DNA ends. By analogy with the enrichment of condensin at highly expressed genes (*22*, *23*), Taz1 bound to telomeres might create an obstacle onto which loop-extruding condensin complexes accumulate in metaphase (Fig. 4D). Such accumulation together with an up-regulation by Aurora-B kinase in anaphase (*10*, *24*) might allow condensin-mediated DNA translocation to pass a threshold beyond which telomere separation takes place.

References and Notes

1. T. Hirano, Condensin-Based Chromosome Organization from Bacteria to Vertebrates. *Cell*. **164**, 847–857 (2016).

2. M. Ganji, I. A. Shaltiel, S. Bisht, E. Kim, A. Kalichava, C. H. Haering, C. Dekker, Real-time imaging of DNA loop extrusion by condensin. *Science*. **360**, 102–105 (2018).

3. M. Kong, E. E. Cutts, D. Pan, F. Beuron, T. Kaliyappan, C. Xue, E. P. Morris, A. Musacchio, A. Vannini, E. C. Greene, Human Condensin I and II Drive Extensive ATP-Dependent Compaction of Nucleosome-Bound DNA. *Mol. Cell*. **79**, 99-114.e9 (2020).

4. J. H. Gibcus, K. Samejima, A. Goloborodko, I. Samejima, N. Naumova, J. Nuebler, M. T. Kanemaki, L. Xie, J. R. Paulson, W. C. Earnshaw, L. A. Mirny, J. Dekker, A pathway for mitotic chromosome formation. *Science*. **359** (2018), doi:10.1126/science.aao6135.

5. T. Gerguri, X. Fu, Y. Kakui, B. S. Khatri, C. Barrington, P. A. Bates, F. Uhlmann, Comparison of loop extrusion and diffusion capture as mitotic chromosome formation pathways in fission yeast. *Nucleic Acids Res.* **49**, 1294–1312 (2021).

6. J. Baxter, N. Sen, V. L. Martinez, M. E. De Carandini, J. B. Schvartzman, J. F. Diffley, L. Aragon, Positive supercoiling of mitotic DNA drives decatenation by topoisomerase II in eukaryotes. *Science*. **331**, 1328–1332 (2011).

7. A. Charbin, C. Bouchoux, F. Uhlmann, Condensin aids sister chromatid decatenation by topoisomerase II. *Nucleic Acids Res.* **42**, 340–348 (2014).

8. E. Piskadlo, A. Tavares, R. A. Oliveira, Metaphase chromosome structure is dynamically maintained by condensin I-directed DNA (de)catenation. *eLife*. **6**, e26120 (2017).

9. A. Clemente-Blanco, N. Sen, M. Mayan-Santos, M. P. Sacristan, B. Graham, A. Jarmuz, A. Giess, E. Webb, L. Game, D. Eick, A. Bueno, M. Merkenschlager, L. Aragon, Cdc14

phosphatase promotes segregation of telomeres through repression of RNA polymerase II transcription. *Nat Cell Biol*. **13**, 1450–6 (2011).

10. C. Reyes, C. Serrurier, T. Gauthier, Y. Gachet, S. Tournier, Aurora B prevents chromosome arm separation defects by promoting telomere dispersion and disjunction. *J. Cell Biol.* **208**, 713–727 (2015).

11. J. Berthezene, C. Reyes, T. Li, S. Coulon, P. Bernard, Y. Gachet, S. Tournier, Aurora B and condensin are dispensable for chromosome arm and telomere separation during meiosis II. *Mol. Biol. Cell*. **31**, 889–905 (2020).

12. X. Robellet, V. Vanoosthuyse, P. Bernard, The loading of condensin in the context of chromatin. *Curr. Genet.* **63**, 577–589 (2017).

13. N. Walther, M. J. Hossain, A. Z. Politi, B. Koch, M. Kueblbeck, Ø. Ødegård-Fougner, M. Lampe, J. Ellenberg, A quantitative map of human Condensins provides new insights into mitotic chromosome architecture. *J. Cell Biol.* **217**, 2309–2328 (2018).

14. T. de Lange, Shelterin-Mediated Telomere Protection. *Annu. Rev. Genet.* **52**, 223–247 (2018).

15. H. A. Wallace, V. Rana, H. Q. Nguyen, G. Bosco, Condensin II subunit NCAPH2 associates with shelterin protein TRF1 and is required for telomere stability. *J. Cell. Physiol.* (2019), doi:10.1002/jcp.28681.

16. J. P. Cooper, E. R. Nimmo, R. C. Allshire, T. R. Cech, Regulation of telomere length and function by a Myb-domain protein in fission yeast. *Nature*. **385**, 744–747 (1997).

17. M. Zofall, D. R. Smith, T. Mizuguchi, J. Dhakshnamoorthy, S. I. S. Grewal, Taz1-Shelterin Promotes Facultative Heterochromatin Assembly at Chromosome-Internal Sites Containing Late Replication Origins. *Mol. Cell*. **62**, 862–874 (2016).

18. T. Uemura, H. Ohkura, Y. Adachi, K. Morino, K. Shiozaki, M. Yanagida, DNA

topoisomerase II is required for condensation and separation of mitotic chromosomes in S. pombe. *Cell*. **50**, 917–25 (1987).

19. Y. Kakui, A. Rabinowitz, D. J. Barry, F. Uhlmann, Condensin-mediated remodeling of the mitotic chromatin landscape in fission yeast. *Nat. Genet.* **49**, 1553–1557 (2017).

20. H. Funabiki, I. Hagan, S. Uzawa, M. Yanagida, Cell cycle-dependent specific positioning and clustering of centromeres and telomeres in fission yeast. *J Cell Biol*. **121**, 961–76 (1993).

21. K. M. Miller, J. P. Cooper, The telomere protein Taz1 is required to prevent and repair genomic DNA breaks. *Mol. Cell*. **11**, 303–313 (2003).

22. H. B. Brandão, P. Paul, A. A. van den Berg, D. Z. Rudner, X. Wang, L. A. Mirny, RNA polymerases as moving barriers to condensin loop extrusion. *Proc. Natl. Acad. Sci. U. S. A.* **116**, 20489–20499 (2019).

23. J. Rivosecchi, D. Jost, L. Vachez, F. D. Gautier, P. Bernard, V. Vanoosthuyse, RNA polymerase backtracking results in the accumulation of fission yeast condensin at active genes. *Life Sci. Alliance*. **4**, e202101046 (2021).

24. K. Tada, H. Susumu, T. Sakuno, Y. Watanabe, Condensin association with histone H2A shapes mitotic chromosomes. *Nature*. **474**, 477–83 (2011).

25. J. Kanoh, M. Sadaie, T. Urano, F. Ishikawa, Telomere binding protein Taz1 establishes Swi6 heterochromatin independently of RNAi at telomeres. *Curr Biol*. **15**, 1808–1819 (2005).

26. S. Moreno, A. Klar, P. Nurse, Molecular genetic analysis of fission yeast Schizosaccharomyces pombe. *Methods Enzym.* **194**, 795–823 (1991).

27. J. Bahler, J. Q. Wu, M. S. Longtine, N. G. Shah, A. McKenzie 3rd, A. B. Steever, A. Wach, P. Philippsen, J. R. Pringle, Heterologous modules for efficient and versatile PCR-based gene targeting in Schizosaccharomyces pombe. *Yeast*. **14**, 943–951 (1998).

28. B. Petrova, S. Dehler, T. Kruitwagen, J. K. Heriche, K. Miura, C. H. Haering, Quantitative

analysis of chromosome condensation in fission yeast. *Mol Cell Biol*. **33**, 984–98 (2013).

29. T. Sutani, T. Yuasa, T. Tomonaga, N. Dohmae, K. Takio, M. Yanagida, Fission yeast condensin complex: essential roles of non-SMC subunits for condensation and Cdc2 phosphorylation of Cut3/SMC4. *Genes Dev*. **13**, 2271–83 (1999).

30. B. Hu, N. Petela, A. Kurze, K.-L. Chan, C. Chapard, K. Nasmyth, Biological chromodynamics: a general method for measuring protein occupancy across the genome by calibrating ChIP-seq. *Nucleic Acids Res.* **43**, e132 (2015).

31. J. Liang, L. Lacroix, A. Gamot, S. Cuddapah, S. Queille, P. Lhoumaud, P. Lepetit, P. G. P. Martin, J. Vogelmann, F. Court, M. Hennion, G. Micas, S. Urbach, O. Bouchez, M. Nöllmann, K. Zhao, E. Emberly, O. Cuvier, Chromatin immunoprecipitation indirect peaks highlight long-range interactions of insulator proteins and Pol II pausing. *Mol. Cell*. **53**, 672–681 (2014).

32. S. S. P. Rao, M. H. Huntley, N. C. Durand, E. K. Stamenova, I. D. Bochkov, J. T. Robinson, A. L. Sanborn, I. Machol, A. D. Omer, E. S. Lander, E. L. Aiden, A 3D map of the human genome at kilobase resolution reveals principles of chromatin looping. *Cell*. **159**, 1665–1680 (2014).

33. N. Sugawara, DNA sequences at the telomeres of the fission yeast S. pombe. (1988).

34. N. Nakazawa, T. Nakamura, A. Kokubu, M. Ebe, K. Nagao, M. Yanagida, Dissection of the essential steps for condensin accumulation at kinetochores and rDNAs during fission yeast mitosis. *J Cell Biol*. **180**, 1115–31 (2008).

35. E. Toselli-Mollereau, X. Robellet, L. Fauque, S. Lemaire, C. Schiklenk, C. Klein, C. Hocquet, P. Legros, L. N'Guyen, L. Mouillard, E. Chautard, D. Auboeuf, C. H. Haering, P. Bernard, Nucleosome eviction in mitosis assists condensin loading and chromosome condensation. *EMBO J.* **35**, 1565–1581 (2016).

36. F. Madeira, Y. M. Park, J. Lee, N. Buso, T. Gur, N. Madhusoodanan, P. Basutkar, A. R. N. Tivey, S. C. Potter, R. D. Finn, R. Lopez, The EMBL-EBI search and sequence analysis tools

APIs in 2019. *Nucleic Acids Res.* **47**, W636–W641 (2019).

Acknowledgments:

We thank the National BioResource-Yeast Project, J. Cooper, JP. Javerzat, M. Yanagida and J. Kanoh for strains; J. Baxter and N. Minchell for teaching the rudiments of Hi-C to L.C., J.P. Javerzat, F. Beckouet, V. Vanoosthuyse and A. Piazza for helpful discussions.

Funding:

L.C. and J.B. are supported by PhD studentships from respectively la Ligue contre le cancer, and a University MRT and la Fondation pour la Recherche Médicale. This work was funded by the CNRS, Inserm (O.C. and S.S.), ANR-blanc120601, ANR-16-CE12-0015-TeloMito and la Fondation ARC (PJA 20191209370 to PB; 20161204921 to ST).

Author contributions:

Conceptualization and Methodology: S.T.; P.B., S.C., Y.G.

Investigation: all authors

Visualization: L.C., C.R., J.B, S.T., P.B., S.C., Y.G.

Funding acquisition: S.T., P.B., S.C., Y.G.

Project administration: S.T.

Supervision: S.T., P.B., S.C., Y.G., O.C.

Writing – original draft: S.T., P.B.

Writing – review & editing: S.T., P.B., S.C., Y.G., O.C.

Competing interests:

Authors declare that they have no competing interests.

Supplementary Materials

Materials and Methods

Supplementary Text

Figs. S1 to S9

References (*26-36*)

Movie S1

Figure Legends

Fig. 1. Taz1 specifically enriches condensin at telomeres. (**A**) The telomere and subtelomere of the right arm of chromosome 2. Subtelomeric-elements (STE), the heterochromatic gene *tlh2*, the domain bound by Taz1 (orange) (*25*) and primers for ChIP-qPCR are shown. (**B**) Cnd2-GFP calibrated ChIP-seq from metaphase arrests at 36°C. Arrows indicate high occupancy binding sites. Mitotic indexes are given in Figure S1A. (**C**) Cnd2-GFP calibrated ChIP-qPCR from metaphase arrests at 30°C. Shown are averages and standard deviations (SD) of mitotic indexes and qPCRs for 3 biological and technical replicates. *cnt1* is the kinetochore domain of *cen1*, *exg1*,

gas1 and *cnd1* are high or low occupancy binding sites on chromosome arms. (**D**) Cnd2-GFP occupancy at non-telomeric Taz1 islands (isl) in the same samples as in (B) and (C), respectively.

Fig. 2. Condensin activity controls telomere disjunction in a decatenation-independent manner during anaphase. (**A-B**) left: live imaging of *cut3-477* or *top2-250* cell undergoing mitosis at 25°C or after a shift at the restrictive temperature using fast microfluidic temperature control. Right: number of telomere foci according to the length of the mitotic spindle (distance between the SPBs). Shown is a representative experiment out of three replicates with n>70 cells, each. (**C**) Left: wild-type cell in anaphase with separated telomeres, and *top2-250* anaphase cell showing telomere disjunction within a chromatin bridge. Right: frequencies of chromatin bridges after 3 hours at the indicated temperatures. Averages and SD obtained from three independent experiments (n=100 cells for each condition) are shown.

Fig. 3. Condensin deficiency increases contact frequencies between telomeres in metaphase. (**A**) Mitotic indexes of cell cultures used for Hi-C. (**B**) Hi-C contact probability matrix at 25 kb resolution of wild-type metaphase arrests at 33°C. Contacts between telomeres (arrows) and centromeres (circles) are indicated. (**C**) Median contact probabilities as a function of distance along chromosomes for wild-type and *cut14-208* metaphases at 33°C. (**D**) Differential Hi-C contact map between wild-type and *cut14-208*. (**E**) Measurements of aggregated of contact frequencies at high resolution (5 kb) over the ends of chromosomes in metaphase arrests at 33°C. Boxes indicate the median, 1st and 3rd quartiles, whiskers the minimum and maximum, and notches represent the 95% confidence interval for each median. Data points are shown as grey circles. The significance in contact frequencies was confirmed statistically by Mann-Whitney-

Wilcoxon test between *cut14-208 and* wild-type conditions.

Fig. 4. Taz1 and condensin act in synergy for telomere disjunction in anaphase. (**A**) Viability test of indicated strains by spotting serial dilutions of cell cultures. (**B**) Live cell analysis of telomere dissociation. (**C**) Micrograph images of two anaphase cells showing a chromatin bridge
5 and telomere non-disjunction. Percentage of chromatin bridges with telomere non-disjunction. Shown are averages and SD calculated from three independent experiments with n=100 cells for each condition. P-values are calculated by a t-test. (**D**) Model for condensin-enrichment at telomeres mediating their disjunction in anaphase, see text for details.

Supplementary Materials for

Condensin positioning at telomeres by the Shelterin protein Taz1 promotes telomere disjunction in anaphase

Léonard Colin [2, 3 †], Céline Reyes[1†], Julien Berthezene[1], Laetitia Maestroni [5], Laurent Modolo [2,3], Esther Toselli [2,3], Nicolas Chanard [1,4], Stephane Schaak[1,4], Olivier Cuvier [1,4], Yannick Gachet [1]*, Stéphane Coulon* [5], Pascal Bernard [2, 3]*, Sylvie Tournier [1]*

[1] MCD, Centre de Biologie Intégrative, Université de Toulouse, CNRS, UPS, 31062 Toulouse Cedex, France"
[2] CNRS - Laboratory of Biology and Modelling of the Cell, UMR 5239, Lyon, France
[3] ENS de Lyon, Univ. Lyon, 46 allée d'Italie, site Jacques Monod, F-69007, Lyon, France
[4] CBI, MCD-UMR5077, CNRS, Chromatin dynamics team, 31062, Toulouse
[5] CNRS, INSERM, Aix Marseille Univ, Institut Paoli-Calmettes, CRCM, Equipe labellisée par la Ligue Nationale contre le Cancer, Marseille, F-13009, France

[†] These authors participate equally to this work.
*Co-corresponding authors: Sylvie Tournier sylvie.tournier-gachet@univ-tlse3.fr , Pascal Bernard pascal.bernard@ens-lyon.fr , Stéphane Coulon stephane.coulon@inserm.fr and Yannick Gachet yannick.gachet@univ-tlse3.fr

This PDF file includes:

Materials and Methods
Supplementary Text
Figs. S1 to S9
Tables S1 to S2
Caption for Movie S1

Other Supplementary Materials for this manuscript include the following:

Movie S1

Materials and Methods

Media, molecular genetics and cell culture

Media, growth, maintenance of strains and genetic methods were as described (*26*). Standard genetics and PCR-based gene targeting method (*27*) were used to construct *S. pombe* strains. All fluorescently tagged proteins used in this study are expressed from single-copy genes under the control of their natural promoters at their native chromosomal locations. Strains used in this study are listed in Table S1. For metaphase arrests used in ChIP and Hi-C experiments, cells expressing the APC/C co-activator Slp1 under the thiamine-repressible promoter *nmt41* (*28*) were cultured in synthetic PMG medium at 30°C, arrested in metaphase for 2h at 30°C by the adjunction of thiamine (20 µM final) and shifted at indicated restrictive temperatures for 1 hour. Mitotic indexes were determined by scoring the percentage of cells exhibiting Cnd2-GFP fluorescence in their nucleoplasm (*29*). For the viability spot assay, cell suspensions of equal densities were serially diluted five-fold and spotted on solid YES medium, the first drop containing 10^7 cells. For microscopy, cells were grown in yeast extract and centrifuged 30 sec at 3000 g before mounting onto an imaging chamber.

Cell imaging and fast microfluidic temperature control experiments

Live cell analysis was performed in an imaging chamber (CoverWell PCI-2.5, Grace Bio-Labs, Bend, OR) filled with 1 ml of 1% agarose in minimal medium and sealed with a 22 × 22-mm glass coverslip. Time-lapse images of Z stacks (maximum five stacks of 0.5 µm steps, to avoid photobleaching) were taken at 30 or 60 sec intervals. Images were acquired with a CCD Retiga R6 camera (QImaging) fitted to a DM6B upright microscope with a x100 1.44NA objective, using MetaMorph as a software. Intensity adjustments were made using the MetaMorph, Image J, and Adobe Photoshop packages (Adobe Systems France, Paris, France). Fast microfluidic temperature control experiments were performed with a CherryTemp from Cherry Biotech. To determine the percentage of chromatin bridges with unseparated telomeres, cells were fixed in 3.7% formaldehyde for 7 min at room temperature, washed twice in PBS, and observed in the presence of DAPI/calcofluor.

Image processing and analysis

The position of the SPBs, kinetochores/centromeres and telomeres were determined by visualization of the Cdc11–CFP, Ndc80–GFP/Mis6-RFP and Taz1-GFP/Ccq1-GFP signals. Maximum intensity projections were prepared for each time point, with the images from each channel being combined into a single RGB image. These images were cropped around the cell of interest, and optional contrast enhancement was performed in MetaMorph, Image J or Photoshop where necessary. The cropped images were exported as 8-bit RGB-stacked TIFF files, with each frame corresponding to one image of the time-lapse series. For both channels, custom peak detection was performed. The successive positions of the SPBs were determined. The number of telomeres during spindle elongation was assessed by eye.

Calibrated-ChIP

Fission yeast cells, expressing either Cnd2-GFP or NLS-GFP, and arrested in metaphase by the depletion of Slp1, were fixed with 1% formaldehyde for 25 min, quenched with glycine 0.125 M final, washed twice with PBS, frozen in liquid nitrogen and stored at -80°C until use. *Saccharomyces cerevisiae* cells expressing Smc3-GFP, used for internal calibration, were grown

in Yeast Peptone Dextrose liquid medium at 30°C in log phase and fixed with 2.5% formaldehyde for 25 min. To perform ChIP, 2.10^8 fission yeast cells were mixed with 4.10^7 budding yeast cells in lysis buffer (50 mM Hepes KOH pH 7.5, NaCl 140 mM, EDTA 1 mM, Triton X-100 1%, sodium deoxycholate 0.1%, PMSF 2mM) supplemented with a protease inhibitor cocktail (cat. 11836170001, Roche). Cells were lysed with Precellys ® and chromatin was sheared to ~ 300 bp fragments with Covaris ® S220 (18 min at duty factor 10%, 200 bursts per cycle, and 140W peak power). Chromatin was clarified twice by centrifugation at 9600 g at 4°C and resuspended in lysis buffer to reach 1 ml final. Two 60 µl aliquots of chromatin each served as Total (input) fractions, while two aliquots of 300 µl of chromatin (IPs) were incubated each with 35 µl of Dynabeads™ protein A (cat. 10002D, Invitrogen) and 8 µg of anti-GFP antibody (cat. A111-22, Invitrogen). Total (T) and IP samples were incubated overnight in a cold room, IPs being put on slow rotation. IPs were washed on a wheel at room temperature for 5 min with buffer WI (Tris-HCl pH8 20 mM, NaCl 150 mM, EDTA 2 mM, Triton X-100 1%, SDS 0.1%), WII (Tris-HCl pH8 20 mM, NaCl 500 mM, EDTA 2 mM, Triton X-100 1%, SDS 0.1%) and WIII (Tris-HCl pH8 10 mM, sodium deoxycholate 0.5%, EDTA 1 mM, Igepal 1%, LiCl 250 mM) and twice with TE pH8 without incubation. Immunoprecipitated materials on beads and Total samples were brought to 100 µl in TE pH8, supplemented with RNAse A at 1µg/µl and incubated 30 min at 37°C. 20 µg of proteinase K was added and tubes were incubated 5h at 65°C. Samples were mixed with Chelex 100 Resin (cat. 142-1253, Biorad) 10% final and incubated 10 min at 98°C, centrifuged and the supernatant was recovered.

For calibrated ChIP-qPCR, real time quantitative (q) PCRs were performed on a Rotor-Gene PCR cycler (Qiagen) using Quantifast (Qiagen) SYBR Green. The ratios (IP/T) calculated for fission yeast DNA sequences where normalized to their associated IP/T ratio calculated for budding yeast CARIV or CEN4 DNA sequences bound by SMC3-GFP. Background IP/T values obtained from the NLS-GFP samples were subtracted to their cognate samples.

For ChIP-seq, Total and IPed DNA were washed with TE pH8 and concentrated using Amicon® 30k centrifugal filters and libraries were prepared using NEBNext® Ultra™ II DNA Library Prep Kit for Illumina® kits according to the manufacturer's instructions. DNA libraries were size-selected using Ampure XP Agencourt beads (A63881) and sequenced paired-end 150 bp with Novaseq S6000 (Novogene®).

Hi-C sample preparation

Fission yeast cells, expressing Cnd2-GFP and arrested in metaphase by the depletion of Slp1 were fixed with 3% formaldehyde for 5 min at 33°C followed by 20 min at 19°C, washed twice with PBS, frozen in liquid nitrogen and stored at -80°C. 2.10^8 cells were lysed in ChIP lysis buffer with Precellys ®. Lysates were centrifuged 5000 g at 4°C for 5 min and pellets were resuspended once in 1 ml lysis buffer and twice in NEB® 3.1 buffer. SDS was added to reach 0.1% final and samples were incubated for 10 min at 65°C. SDS was quenched on ice with 1% Triton X-100 and DNA digested overnight at 37°C with 200 Units of *Dpn*II restriction enzyme. Samples were incubated at 65°C for 20 min to inactivated *Dpn*II. Restricted-DNA fragments were filled-in with 15 nmol each of biotin-14-dATP (cat. 19524016, Thermofisher), dTTP, dCTP and dGTP, and 50 units of DNA Klenow I (cat. M0210M, NEB) for 45 min at 37°C. Samples were diluted in 8 ml of T4 DNA ligase buffer 1X and incubated 8 hours at 16°C with 8000 Units of T4 DNA ligase (NEB). Crosslinks were reversed overnight at 60°C in the presence of proteinase K (0.125 mg / ml final) and SDS 1% final. 1 mg of proteinase K was added again and tubes were further incubated for 2 hours at 60°C. DNA was recovered by phenol-chloroform-isoamyl-alcohol extraction, resuspended in 100 µl TLE (Tris/HCl 10 mM, 0.1 mM EDTA, pH8) and treated with RNAse A

(0.1 mg / ml) for 30 min at 37°C. Biotin was removed from unligated ends with 3 nmol dATP, dGTP and 36 Units of T4 DNA polymerase (NEB) for 4 hours at 20°C. Samples were incubated at 75°C for 20 min, washed using Amicon® 30k centrifugal filters and sonicated in 130 µl H_2O using Covaris® S220 (4 min 20°C, duty factor 10%, 175W peak power, 200 burst per cycle). DNA was end-repaired with 37.5 nmol dNTP, 16.2 Units of T4 DNA polymerase, 54 Units of T4 polynucleotide kinase, 5.5 Units of DNA Pol I Klenow fragment for 30 min at 20°C and then incubated for 20 min at 75°C. Ligated junctions were pulled-down with Dynabeads® MyOne™ Streptavidin C1 beads for 15 min at RT and DNA ends were A-tailed with 15 Units of Klenow exo- (cat. M0212L, NEB). Barcoded PerkinElmer adapters (cat. NOVA-514102) were ligated on fragments for 2 hours at 22°C. Libraries were amplified with NextFlex PCR mix (cat. NOVA-5140-08) for 5 cycles, and cleaned up with Ampure XP Agencourt beads (A63881). Hi-C libraries were paired-end sequenced 150bp on Novaseq6000.

Calibrated ChIP-seq data analysis

Scripts and pipelines are available in the git repository gitbio.ens-lyon.fr/LBMC/Bernard/condensin_cal_ChIPseq. Pipelines were executed with `nextflow` (version 21.10.6.5660). In the subsequent section, *genome* refers to the *S. pombe* genome (ASM294v2, or its TEL2-R extended version) while *calibration genome* refers to the genome of *S. cerevisiae* (sacCER3 release R64-1-1) used for internal calibration. We start by processing the fastq file with `fastp` (version 0.20.1). Then we concatenate the genome and the calibration genome and prefix every chromosome in the calibration genome with the string `calib_`. The processed fastq files are then mapped on the concatenated genome with `bowtie2` (versio 2.3.4.1). The resulting bam files were then sorted and indexed with `samtools` (version 1.11), before being split into bam of reads mapping exclusively on the genome and bam of reads mapping exclusively on the calibration genome with samtools and awk. We then removed duplicated reads with `picard` (version 2.18.11). The bam files were then converted to bigwig and bedgraph formats using `deeptools` (version 3.5.1). Read numbers were normalized according the method of Hu et al. (*30*). For each bedgraph file, we computed $normIP_{xt}$ as the normalized read density in the IP fraction at position t of the genome by applying the following transformation:

$$\text{norm}IP_i(t) = IP_{xi}(t)\frac{10^6 \sum_{t=1}^{T_c} W\,CE_{ci}(t)}{\sum_{t=1}^{T_c} I\,P_{ci}(t) \sum_{t=1}^{T_x} W\,CE_{xi}(t)}$$

With $IP_{xi}(t)$, the read density at position t in the genome of size T_x, and $IP_{ci}(t)$, the read density at position t in the calibration genome of size T_c for the IP sample i, and $WCE_{xi}(t)$ and $WCE_{ci}(t)$ the read density for the corresponding WCE (Whole Cell Extract, i.e. Total or Input) sample i. To analyze the coverage information at repetitive regions of the genome, we calculated the IP/WCE ratio for each base with the following quantity:

$$\text{ratio}IP_i(t) = \frac{\text{norm}IP_i(t)}{\text{norm}WCE_i(t)}$$

with:

$$\text{norm}WCE_{i(t)} = WCE_{xi}(t)\frac{10^6}{\sum_{t=1}^{T_c} W\,CE_{ci}(t)}\alpha_i$$

We then find α_i such that:

$$E\big(\text{norm}IP_i(t)\big) = E\left(\frac{\text{norm}IP_i(t)}{\text{norm}WCE_i(t)}\right)$$

$$\frac{1}{T_x}\sum_{t=1}^{T_x}\text{norm}\,IP_i(t) = \frac{1}{T_x}\sum_{t=1}^{T_x}\left(\frac{\text{norm}IP_i(t)}{\text{norm}WCE_i(t)}\right)$$

$$\sum_{t=1}^{T_x}\text{norm}\,IP_i(t) = \sum_{t=1}^{T_x}\left(\frac{\text{norm}IP_i(t)}{WCE_{xi}(t)\dfrac{10^6}{\sum_{t=1}^{T_c} W\,CE_{ci}(t)}\alpha_i}\right)$$

$$\alpha_i = \frac{\sum_{t=1}^{T_x}\left(\dfrac{\text{norm}IP_i(t)}{WCE_{xi}(t)\dfrac{10^6}{\sum_{t=1}^{T_c} W\,CE_{ci}(t)}}\right)}{\sum_{t=1}^{T_x}\text{norm}\,IP_i(t)}$$

With E, the expected value, or weighted average. This method conserves the normalization on the average read density between samples (i.e., we can compare two different samples in a quantitative way) and we account for the local bias of read density in the WCE/Total samples.

Hi-C data analysis

Computational analyses of Hi-C data were performed with R (version 3.4.3). Reads were aligned on the genome of S. pombe version ASM294v2 using bwa (version 0.7.17-r1188) with default settings. Hi-C contacts matrices of DpnII digested genomic fragments were normalized and processed using Juicer (version 1.6: https://github.com/aidenlab/juicer). Hi-C reads were binned to a resolution of 5 kb using a square root vanilla count normalization. 2D plots were performed for normalized (observed/expected) Hi-C read counts using Juicebox. Differential 2D plots were visualized in Log2 (of normalized Hi-C reads in mutants / normalized Hi-C reads in wild-type control). Aggregation of Hi-C data was performed essentially as previously described (*31*, *32*) with the following modified parameters for adaptation to 3D contacts at telomeres: Hi-C reads were counted over bins of 5 kb over a 150 kb distal region covering both telomeres of each chromosome. Long-range interactions were assessed for all combinations of telomeres over a sliding matrix (21x21 bins). To optimize detection of long-range interactions between telomeres, a quantilization was performed by ranking the 21x21 bins of every sub-matrix contributing to the aggregation, allowing to assess interactions from averaged values. Statistical analyses were performed both for the corresponding quantilized matrices, and verified with non-quantilized matrices, using a Mann-Whitney-Wilcoxon test using R (Stats4) and validated for each of the replicates made for every mutant and wild-type conditions.

Telomere length analysis by Southern blotting

Genomic DNA was prepared and digested with *Apa*I. The digested DNA was resolved in a 1.2% agarose gel and blotted onto a Hybond-XL membrane. After transfer, DNA was crosslinked to the membrane with UV and hybridized with a radiolabelled telomeric probe. The telomeric DNA probe was extracted by digestion of pIRT2-Telo plasmid by *Sac*I/*Pst*I.

Supplementary Text

Fission yeast condensin is mostly localized in the cytoplasm during interphase and imported into the nucleus during mitosis (*29*). To assess condensin localization at telomeres, cells were blocked in metaphase by the depletion of the APC co-activator Slp1/Cdc20 (*28*) and processed for calibrated ChIP-sequencing (ChIP-seq) against Cnd2-GFP. The current version of the fission yeast genome lacking telomere-proximal DNA and telomere repeats, to map ChIP-seq reads at telomeres, we generated a version containing a full-length telomere 2 right (TEL2R) sequence (Fig. S2). Furthermore, since subtelomeres and telomeres contain repeated DNA sequences (*33*), we determined Cnd2-GFP occupancy by calculating, at each base, the ratio of calibrated read-counts between the immunoprecipitated (IP) and Total (T) fractions (Materials and Methods). As shown in Figure S3 using pericentric DNA repeats and rDNA repeats as examples, IP/T ratios correct for biases in coverage in the Total fractions, and produces ChIP-seq profiles that are more consistent with previously published ChIP-qPCR analyses (*34*, *35*). This method has been used to assess Cnd2-GFP occupancy at telomeres repeats in wild-type and *cut3-477* mutant cells (Fig. 1).

Fig. S1, related to Fig. 1. The *cut3-477* mutation reduces condensin binding genome-wide at the restrictive temperature. Wild-type or *cut3-477* mutant cells expressing Cnd2-GFP were arrested in metaphase at 30°C, shifted at 36°C for 1 hour to inactivate the thermosensitive Cut3-477 condensin subunit and processed for calibrated ChIP-seq against Cnd2-GFP using budding yeast cells expressing SMC3-GFP for calibration, with n = 2 biological and technical replicates (Rep.). (**A**) Averages and standard deviations of the mitotic indexes of cell cultures. (**B**) Calibrated read counts at centromere 2 (*cen2*) and at neighbouring high occupancy condensin binding sites along chromosome arms. (**C**). Metagene profiles of high-occupancy condensin binding sites along chromosome arms; TSS (transcription Start Site), TTS (Transcription Termination Site).

Fig. S2, related to Fig. 1. Construction of a version of the fission yeast genome containing a full-length telomere 2 right. (**A**) Telomeric plasmid pNSU70 (*33*) aligned against the current ASM294v2 version of the *S. pombe* genome using Blast shows a best hit with the right end of chromosome 2. (**B**). Cosmid SPBCT2R1 corresponding to the right end of chromosome 2 (nucleotides 4500619 to 4539800) was aligned with pNSU70 using Clustal Omega (*36*). Nucleotides 4137 to 7223 of pNSU70 were added to chromosome 2 to create a TEL2R-extended version of the genome available under the accession number GSE196149.

Fig. S3, related to Fig. 1. Base per base ratios of calibrated ChIP-seq signals corrects for biases in coverage. (**A**) Overview of the base per base normalization method applied to correct for biases in coverage in the IP and Total (Input) fractions. (**B**) Calibrated read counts at centromere 2 (*cen 2*), composed of a central core (cc) flanked by repetitive heterochromatic outer repeats (otr) and at rDNA repeats. The single-copy gene *exg1* serves as a non-repetitive control. Mappings have been done on the TEL2R-extented-ASM294v2 version of fission genome. Shown are the results of two biological and technical replicates (Rep.).

Fig. S4, related to Fig. 1. Condensin is enriched at telomere repeats in a Taz1-dependent manner. (A) Calibrated ChIP-seq read counts from two biological and technical replicates (Rep.). Data from Rep. 1 are also shown in Figure 1. Shown are the normalized read-counts form the ChIP (IP) and Total (T) fractions, and the corresponding base per base IP/T ratios. (**B**) Cnd2-GFP calibrated ChIP-qPCR shown in Figure 1C were normalized with respect to their corresponding IP/T ratios of budding SMC3-GFP at CEN4. *cnt1* is the kinetochore domain of *cen1*, *exg1*, *gas1* and *cnd1* are high or low occupancy binding sites on chromosome arms. Shown are the average and standard deviations from n=3 biological and technical replicates.

Fig. S5 related to Fig. 1. Condensin is not enriched at non-telomeric Taz1 islands. Cnd2-GFP occupancy at non-telomeric Taz1 islands in wild-type or *cut3-477* mutant cells arrested in metaphase, as determined by calibrated ChIP-seq data of Cnd2-GFP (n =2 biological and technical replicates). Calibrated ChIP-seq samples are the same as shown in Figures 1 and S4. Table summarize the results obtained at all known Taz1 islands (*17*).

Fig. S6 related to Fig. 2. Condensin activity controls telomere disjunction in a decatenation-independent manner during anaphase. (**A**) *cut14-90* and (**B**) *cut14-208* condensin mutants were grown at the restrictive temperature of 36°C for three hours, fixed with formaldehyde and observed in the presence of DAPI and Calcofluor to stain DNA and the septum, respectively. Telomeres are

visualized via Taz1-GFP (green), kinetochores/centromeres via the co-localization of the Ndc80-GFP (green) and Mis6-RFP (red) signals, and SPBs via Cdc11-CFP (blue). Right panels. Number of telomere foci according to the distance between SPBs in condensin mutants at 36°C compared to WT at 36°C. The data shown are from a single representative experiment out of three repeats. For the experiment shown, n>70 cells for each condition. (**C**) Kymograph representation of kinetochore dynamics in live *top2-250* mutant cells at permissive temperature (25°C) or restrictive temperature (18°C). Kinetochores are visualized via Ndc80-GFP (green) and SPBs via Cdc11-CFP (red). Right panel. Quantification of the percentage of *top2-250* anaphase cells showing lagging centromeres. Error bars indicate SD obtained from three independent experiments (n=100 for each condition). (**D**). Percentage of anaphase cells displaying chromatin bridges in wild-type (grey), *top2-250* (brown), *cut14-208* (green), or *cut14-90* (purple) cells grown at the permissive or restrictive temperature for 3 hours. Error bars indicate SD obtained from three independent experiments (n=100 for each condition).

Fig. S7, related to Fig. 3. Condensin deficiency increases contact frequencies between telomeres in metaphase. Data from the biological and technical replicate of those shown Fig. 3. (**A**) Mitotic indexes of cell cultures used for Hi-C. (**B**) Hi-C contact probability matrix at 25 kb resolution of wild-type cells arrested in metaphase at 33°C. Contacts between telomeres (arrows) and centromeres (circles) are indicated (**C**) Median contact probabilities as a function of distance along the chromosomes for wild-type and cut14-208 cells arrested in metaphase at 33°C. (**D**) Hi-C difference map at 25 kb resolution comparing *cut14-208* and wild-type cells. (**E**) Aggregation of contact frequencies at chromosome ends in wild-type and cut14-208 mutant cells in metaphase at 33°C. Boxes indicate the median, 1st and 3rd quartiles, whiskers extend to minimum and maximum values and notches represent the 95% confidence interval for each median. Data points are shown as grey circles.

Fig. S8, related to Fig. 4. Taz1 and condensin act in synergy for telomere disjunction in anaphase. (**A-D**) Micrographs from video-microscopy analysis of telomere dissociation in live cells following temperature shift at 32°C for 2 hours: (A) wildtype, (B) *taz1*Δ, (C) *cut3-477*, (D) *cut3-477 taz1*Δ. (**E-F**) Single cell analysis of movies corresponding to A-D, illustrating the number of detectable Ccq1-GFP foci (green curve) according to spindle length (black curve). The data shown are from a single representative movie out of three experimental repeats (n>10 movies for each experiment).

Fig. S9. Mutations in condensin lead to variations in telomere length. (**A**) Relative position of the restriction sites in the telomeric and subtelomeric regions of *S. pombe* chromosomes based on pNSU70 plasmid. The telomeric probe is represented by a red bar. (**B**) Genomic DNA from the indicated strains at the indicated temperatures was digested with *Apa*I and Southern blotted. The membrane was hybridized with the telomeric probe that reveals telomeric signal. The relative gain or loss of telomeric DNA compare to WT is indicated.

Table S1. Strain list used in this study

Strain	genotype	Figures
LY6281	*Mata ade2-1 his3-11 his3-15 ura3 leu2-3 trp1-1 can1-100 SMC3-GFP-KanR*	Fig. 1, S1, S3, S4A, S5
LY5480	*h? leu1-32 ura4D-18 ade6-21? ura4-Pnmt41-slp1+ aur1::pad421-NLS-GFP-9PK::aur1R*	Fig. 1C-D, S4B
LY4483	*h- leu1-32 ura4D-18 ura4-Pnmt41-slp1+ cnd2-*	Fig. 1, 3, S1, S3, S4, S5, S7

	GFP-LEU2	
LY6304	*h+ leu1-32 ura4D cut3-477 ura4-Pnmt41-slp1+ cnd2-GFP-LEU2*	Fig. 1, S1, S3, S4A, S5
LY6305	*h- leu1-32 ura4D cut14-208 ura4-Pnmt41-slp1+ cnd2-GFP-LEU2*	Fig. 3 & S7
LY5298	*h? leu1-32 ura4D18 ade6-21? KanR-Pnmt1-slp1+ taz1Δ::ura4+ cnd2-GFP-LEU2*	Fig. 1C-D, S4B
LY5948	*h- leu1-32 ura4D ura4-Pnmt41-slp1+ rap1Δ::KanR cnd2-GFP-LEU2*	Fig. 1C-D, S4B
ST2229	*h? cdc11-CFP::KanR taz1-GFP:: KanR*	Fig. 2C & Fig. S6A-B
ST2222	*h? cut3-477 cdc11-CFP::KanR taz1-GFP:: KanR*	Fig. 2A
ST1665	h? *top2-250 cdc11-CFP:: KanR taz1-GFP:: KanR*	Fig. 2B
PR109	*h- leu1-32 ura4D-18*	Fig. 4A, S9B
SC388	*h- leu1-32 ura4D-18 ade6-M210 taz1 ::ura4+*	Fig. 4A
LY999	*h- leu1-32 ura4D ade6-M210 cut3-477 :NatR*	Fig. 4A, S9B
SC1432	*h ? leu1-32 ura4D-18 taz1::ura4+ cut3-477 :NatR*	Fig. 4A
ST1928	*h? taz1::ura+ cut3-477 ccq1-GFP::KanR cdc11-CFP:: KanR ura4D-18*	Fig. 4B-C & Fig. S8
ST1645	*h+ cut14-90 taz1-GFP::KanR ndc80-GFP cdc11-CFP::KanR mis6-2mRFP::hph*	Fig. S6A & movie S1
ST1737	*h? cut14-208 taz1-GFP::KanR ndc80-GFP cdc11-CFP::KanR mis6-2mRFP::hph*	Fig. S6B
ST1664	h? *top2-250 ndc80-GFP:: KanR cdc11-CFP:: KanR mis6-RFP-hyg*	Fig. S6C
ST1172	*h? ccq1-GFP:: KanR cdc11-CFP:: KanR*	Fig. 4B-C & Fig. S8
ST1183	*h- taz1::KanR ccq1-GFP::KanR cdc11-CFP:: KanR*	Fig. 4B-C & Fig. S8
ST1657	*h- cut3-477 ccq1-GFP:: KanR cdc11-CFP :: KanR*	Fig. 4B-C & Fig. S8
LY646	*h- leu1-32 ura4D-18 cut14-90*	Fig. S9B
LY140	*h- leu1-32 ura4D cut14-208*	Fig. S9B
LY1252	*h- leu1-32 ura4D ade6-M210 cut14-180*	Fig. S9B
LY3185	*h- ura4D ade6-M210 cut3-M26*	Fig. S9B

LY3186 *h- ura4D ade6-M210 cut3-I23-GFP:his7+* Fig. S9B

Table S2. Primers used for qPCR

Site	Forward primer	Reverse primer
cnt1	ACCGTTGCAACTTACATCAGC	GGTCGCCAAATAGCAATGAG
exg1	CACATAGACGGACCACTTTGAG	ATATGTCACCTGTGGCTGAGTG
gas1	AATAGCATGTCGAGGTTGTATGG	TGTCATCGCGAAACCTTACC
cnd1	AGCAATTAGCCGAACGTCTG	CACCACATGATCCCATTGAC
tel19	CGGGATAACACACATGCAAC	GCTTTGATGGCAACTGGTTC
tel13	CCAATCCCCAGGTTTCTTTC	TTTCGACCTATCAGCGGTTG
tel9.2	ACACGCTCTGACAACATTCG	CGCAATCTCGATTACCGAAC
tel6.1	AAACAACTGCAAGCGGTAGG	CGCATTTACCATTCCTCCAC
tel2.4	AGCAGGGGACTATATTGGAGTG	CCCCTTCAATTACCAAAGTCCAC
tel0	GTGTGGAATTGAGTATGGTGAA	CGGCTGACGGGTGGGGCCCAA TA
isl7	ACACTTGTTTCAGCCGATTTC	AAGCATTGCTCCATTAAAACAAC
isl13	ATGAAGGTACGGAAGCAACG	TAGCCCTTTCATTAATAGCTTCG
isl15	AGAAAAGGCAATGCGAGAGC	CGCAAATCATCTGACATTGG
scCARIV	TCAGGGAAGGTACGGAAATG	GCATGACTATTCGCGTTTGAG
scCEN4	AAATGCCGAGGCTTTCATAG	GTGACGATAAAACCGGAAGG

Movie S1: Fluorescent time-lapse imaging of telomeres and centromeres dynamics in the condensin mutant *cut14-90* at non-permissive temperature.

Movie of a *cut14-90* cell at 36°C expressing Taz1-gfp (telomeres, green), Ndc80-GFP (Kinetochores, green), Mis6-RFP (centromeres, red) and Cdc11-GFP (SPBs, blue). Frames were taken every 30 seconds (7 Z stacks). Note the defect in telomere separation while centromeres/kinetochores are correctly segregating toward the spindle poles.

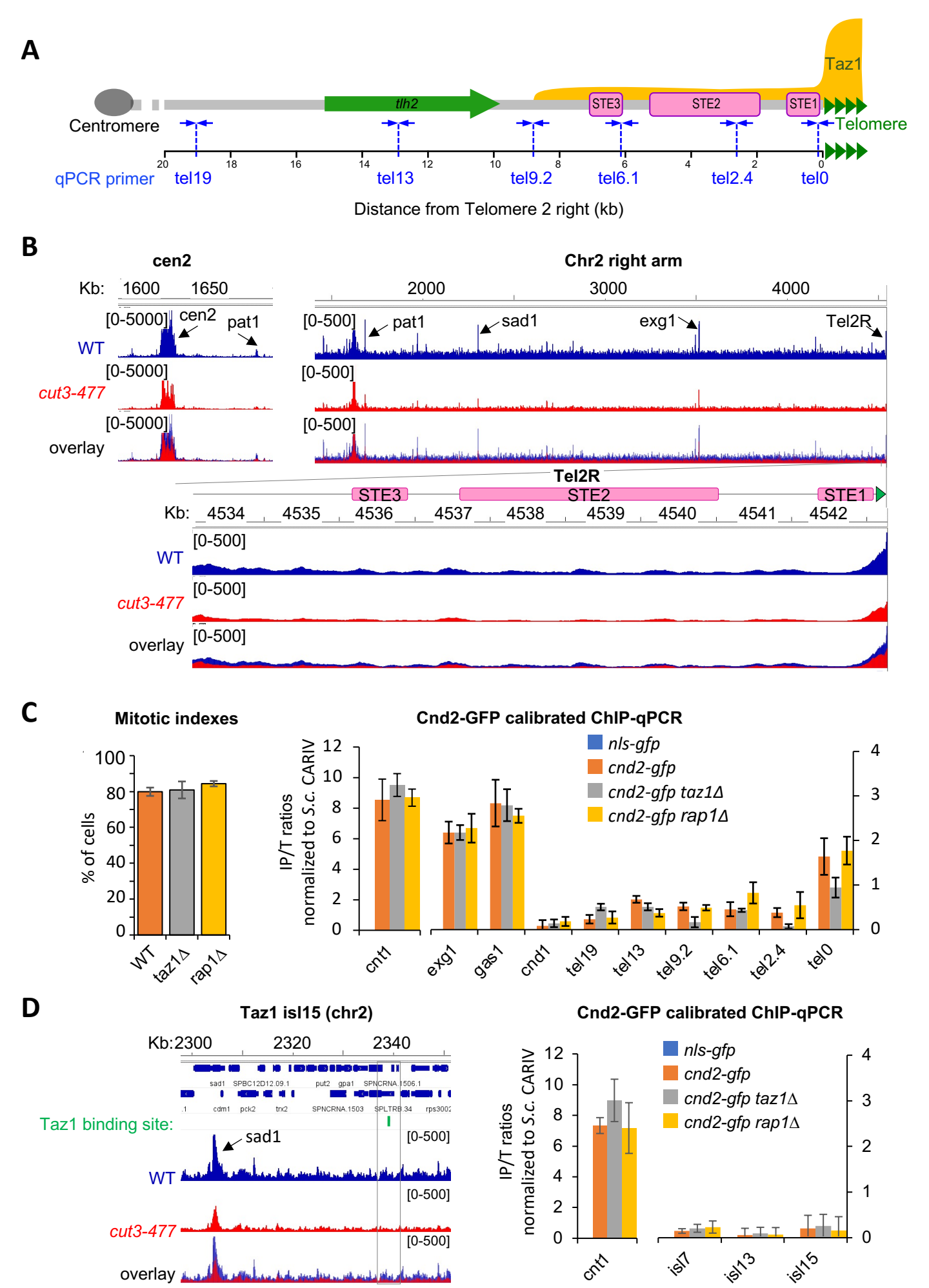
A
Taz1
tlh2
STE3
STE2
STE1
Centromere
Telomere
qPCR primer
tel19
tel13
tel9.2
tel6.1
tel2.4
tel0
Distance from Telomere 2 right (kb)
B
cen2
Chr2 right arm
Kb:
1600
1650
2000
3000
4000
[0-5000]
cen2
pat1
[0-500]
pat1
sad1
exg1
Tel2R
WT
cut3-477
overlay
Tel2R
STE3
STE2
STE1
4534
4535
4536
4537
4538
4539
4540
4541
4542
C
Mitotic indexes
% of cells
WT
taz1Δ
rap1Δ
Cnd2-GFP calibrated ChIP-qPCR
IP/T ratios normalized to S.c. CARIV
nls-gfp
cnd2-gfp
cnd2-gfp taz1Δ
cnd2-gfp rap1Δ
cnt1
exg1
gas1
cnd1
tel19
tel13
tel9.2
tel6.1
tel2.4
tel0
D
Taz1 isl15 (chr2)
Kb:2300
2320
2340
Taz1 binding site:
sad1
[0-500]
WT
cut3-477
overlay
Cnd2-GFP calibrated ChIP-qPCR
IP/T ratios normalized to S.c. CARIV
nls-gfp
cnd2-gfp
cnd2-gfp taz1Δ
cnd2-gfp rap1Δ
cnt1
isl7
isl13
isl15

Figure 1

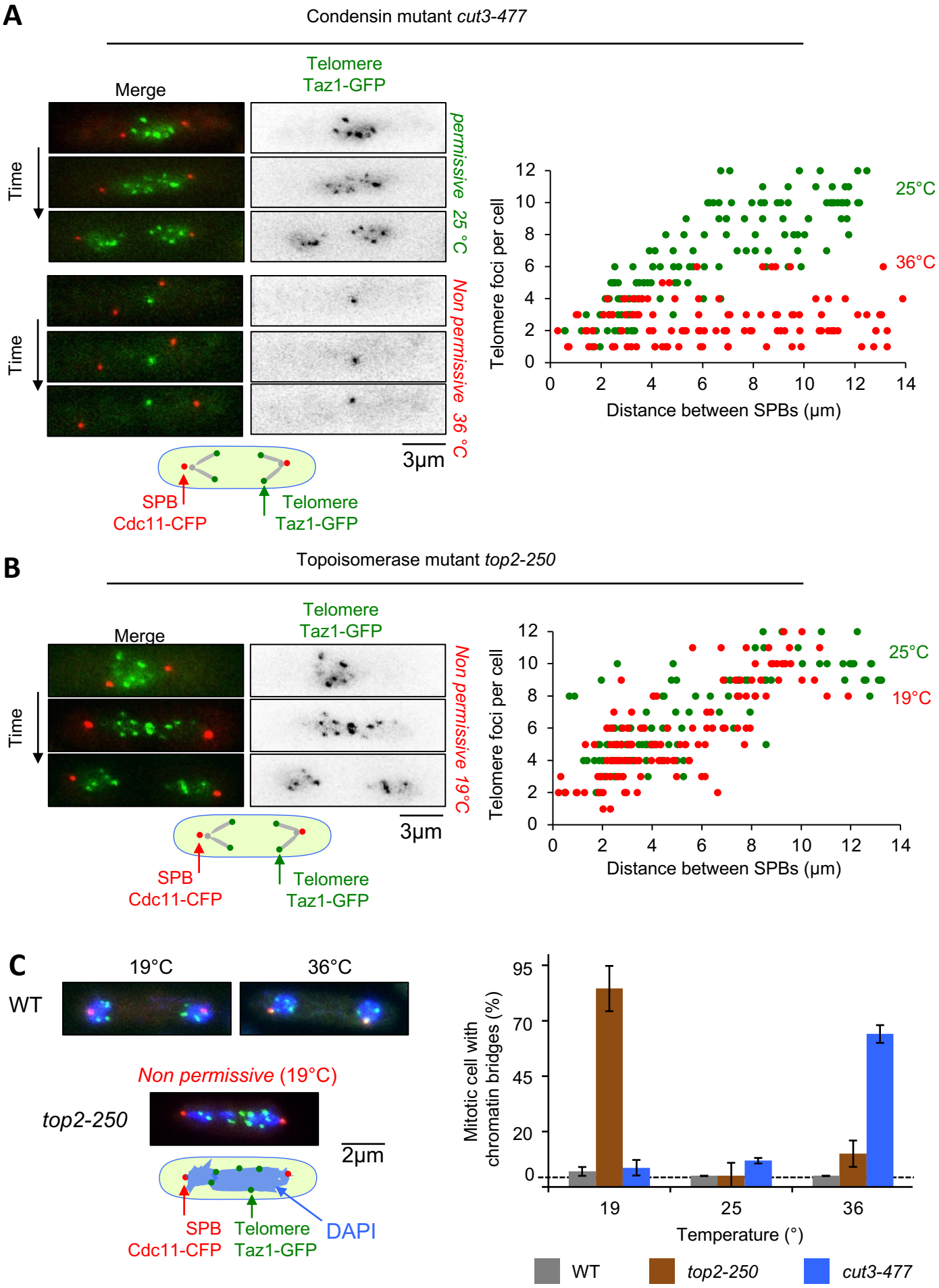
A
Condensin mutant cut3-477
Merge
Telomere
Taz1-GFP
Time
permissive 25 °C
Non permissive 36 °C
3µm
SPB
Cdc11-CFP
Telomere
Taz1-GFP
Telomere foci per cell
Distance between SPBs (µm)
25°C
36°C
B
Topoisomerase mutant top2-250
Non permissive 19°C
19°C
C
WT
19°C
36°C
Non permissive (19°C)
top2-250
2µm
DAPI
Mitotic cell with chromatin bridges (%)
Temperature (°)
WT
top2-250
cut3-477

Figure 2

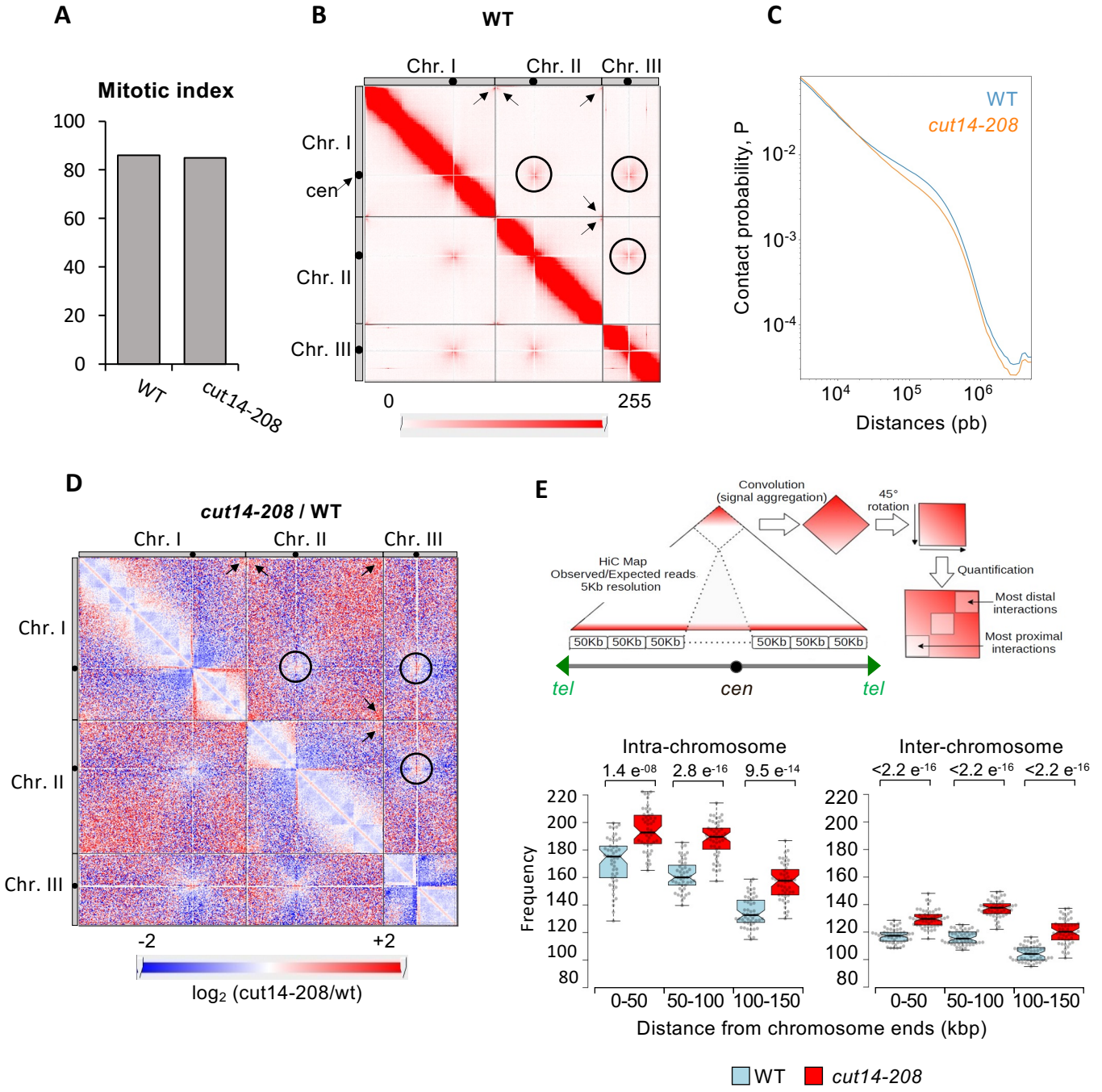
A
Mitotic index
100
80
60
40
20
0
WT
cut14-208
B
WT
Chr. I
Chr. II
Chr. III
cen
0
255
C
WT
cut14-208
Contact probability, P
10^{-2}
10^{-3}
10^{-4}
10^{4}
10^{5}
10^{6}
Distances (pb)
D
cut14-208 / WT
Chr. I
Chr. II
Chr. III
-2
+2
log_2 (cut14-208/wt)
E
Convolution
(signal aggregation)
45°
rotation
Quantification
HiC Map
Observed/Expected reads
5Kb resolution
50Kb
Most distal
interactions
Most proximal
interactions
tel
cen
tel
Intra-chromosome
1.4 e^{-08}
2.8 e^{-16}
9.5 e^{-14}
Inter-chromosome
<2.2 e^{-16}
<2.2 e^{-16}
<2.2 e^{-16}
Frequency
220
200
180
160
140
120
100
80
0-50
50-100
100-150
Distance from chromosome ends (kbp)
WT
cut14-208

Figure 3

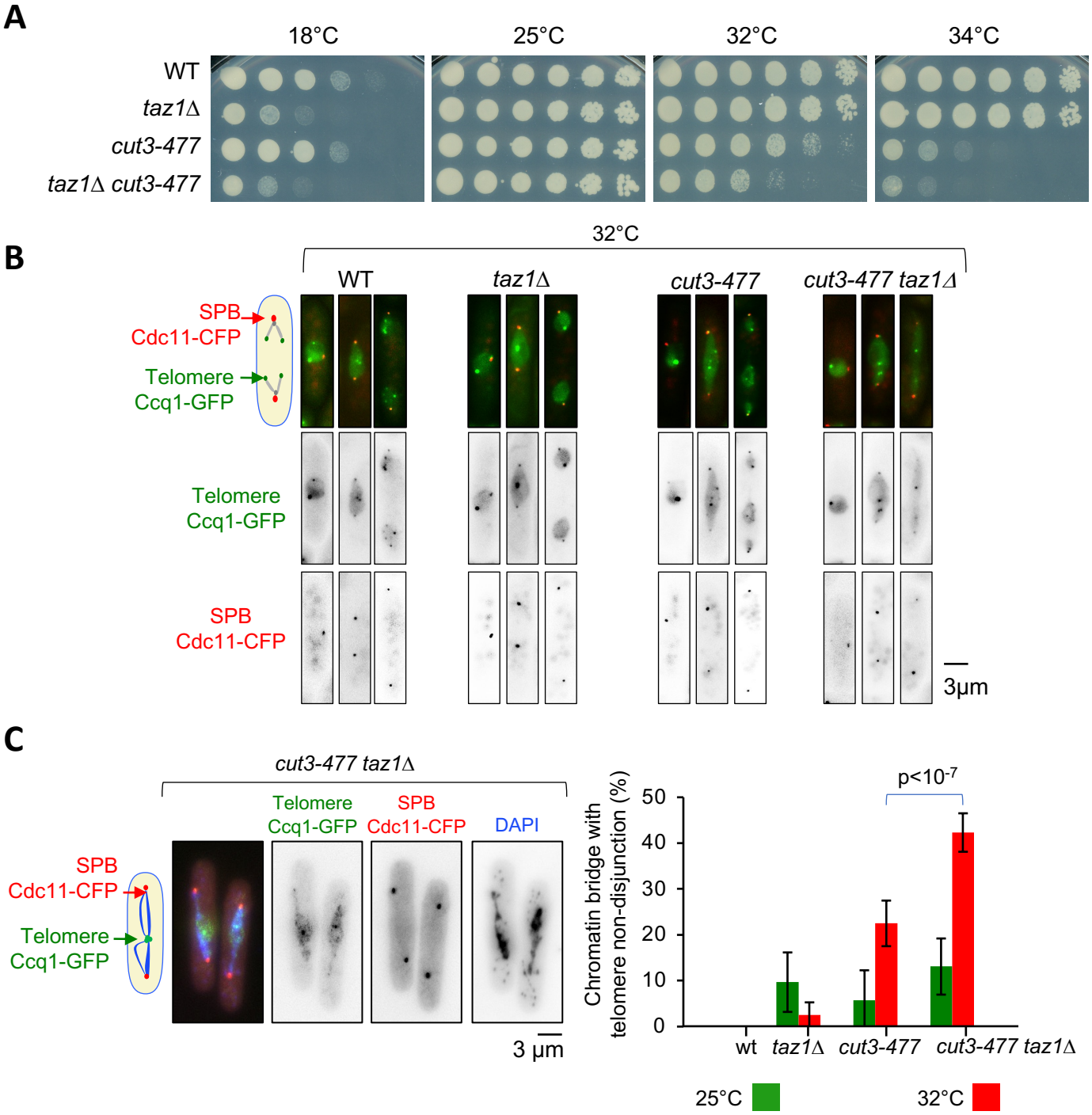
A
18°C
25°C
32°C
34°C
WT
taz1Δ
cut3-477
taz1Δ cut3-477
B
32°C
WT
taz1Δ
cut3-477
cut3-477 taz1Δ
SPB
Cdc11-CFP
Telomere
Ccq1-GFP
Telomere
Ccq1-GFP
SPB
Cdc11-CFP
3μm
C
cut3-477 taz1Δ
Telomere
Ccq1-GFP
SPB
Cdc11-CFP
DAPI
SPB
Cdc11-CFP
Telomere
Ccq1-GFP
3 μm
Chromatin bridge with telomere non-disjunction (%)
p<10-7
50
40
30
20
10
0
wt
taz1Δ
cut3-477
cut3-477 taz1Δ
25°C
32°C

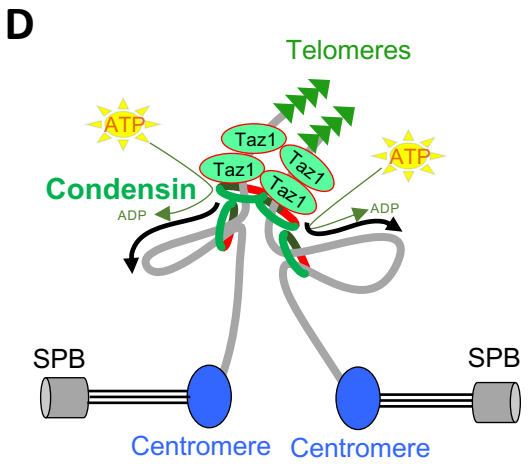
D
Telomeres
ATP
Taz1
Taz1
Taz1
Taz1
ATP
Condensin
ADP
ADP
SPB
SPB
Centromere
Centromere

Figure 4

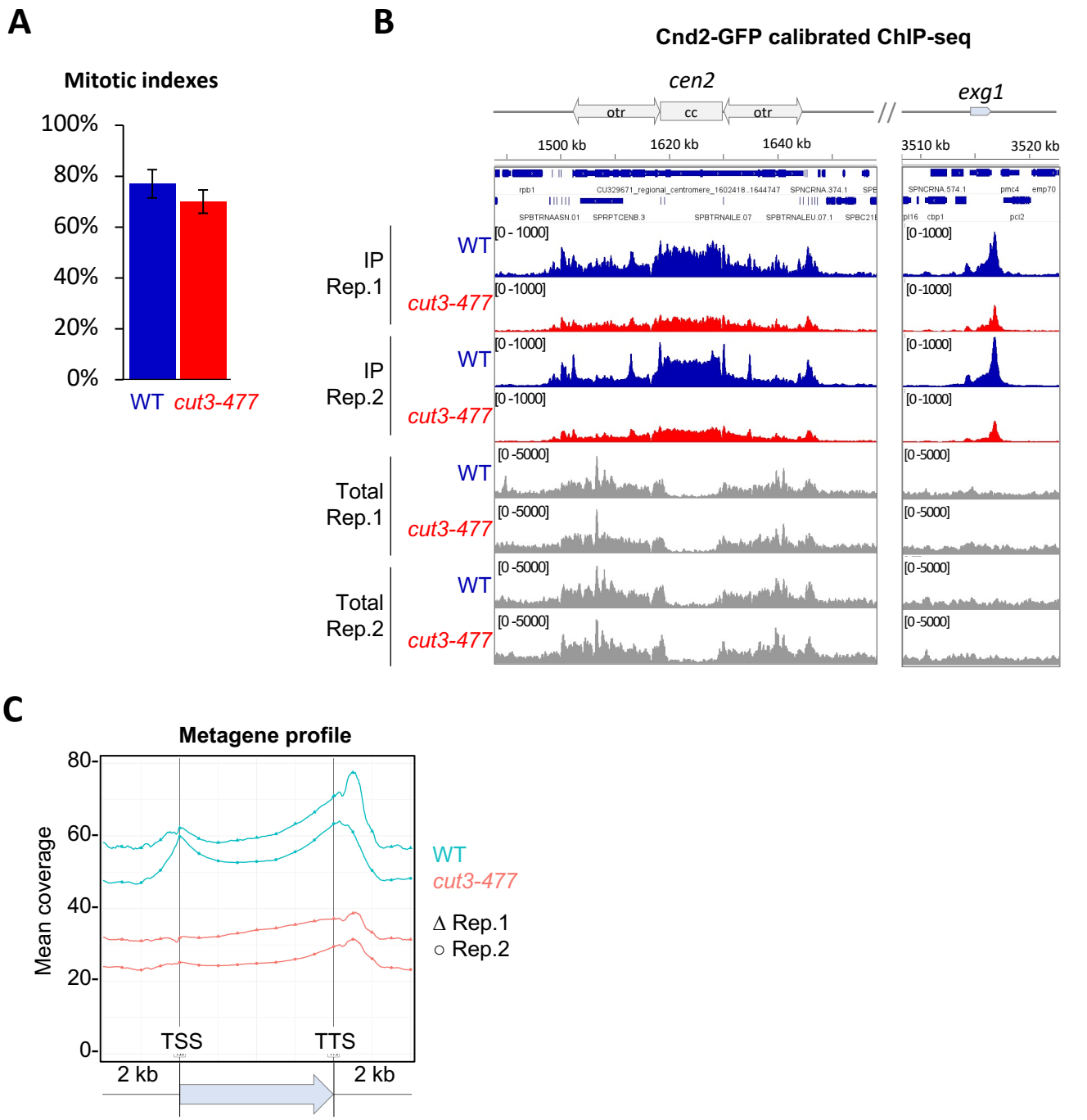

Fig. S1, related to Fig. 1. The *cut3-477* mutation reduces condensin binding genome-wide at the restrictive temperature. Wild-type or *cut3-477* mutant cells expressing Cnd2-GFP were arrested in metaphase at 30°C, shifted at 36°C for 1 hour to inactivate the thermosensitive Cut3-477 condensin subunit and processed for calibrated ChIP-seq against Cnd2-GFP using budding yeast cells expressing SMC3-GFP for calibration, with n = 2 biological and technical replicates (Rep.). (**A**) Averages and standard deviations of the mitotic indexes of cell cultures. (**B**) Calibrated read counts at centromere 2 (*cen2*) and at neighbouring high occupancy condensin binding sites along chromosome arms. (**C**). Metagene profiles of high-occupancy condensin binding sites along chromosome arms; TSS (transcription Start Site), TTS (Transcription Termination Site).

A

Blast pNSU70 against S. pombe genome

Genomic location	Orientation	Length	Score	E-val	%ID
II:4537396-4539804 [Sequence]	Forward	2409 [Sequence]	2409	0.0	100.0 [Alignment]
II:4535663-4537215 [Sequence]	Forward	1553 [Sequence]	1553	0.0	100.0 [Alignment]
II:4537650-4538045 [Sequence]	Forward	396 [Sequence]	392	0.0	99.7 [Alignment]
II:4538576-4538971 [Sequence]	Forward	396 [Sequence]	392	0.0	99.7 [Alignment]
II:4538324-4538661 [Sequence]	Forward	338 [Sequence]	318	1.1e-179	98.5 [Alignment]
II:4539257-4539594 [Sequence]	Forward	338 [Sequence]	318	1.1e-179	98.5 [Alignment]
II:4537727-4537944 [Sequence]	Forward	218 [Sequence]	206	7.6e-113	98.6 [Alignment]
II:4538653-4538870 [Sequence]	Forward	218 [Sequence]	206	7.6e-113	98.6 [Alignment]
II:4539572-4539789 [Sequence]	Forward	218 [Sequence]	206	7.6e-113	98.6 [Alignment]
II:4539572-4539789 [Sequence]	Forward	218 [Sequence]	206	7.6e-113	98.6 [Alignment]
II:4537214-4537408 [Sequence]	Forward	195 [Sequence]	191	6.8e-104	99.5 [Alignment]
I:5571243-5571425 [Sequence]	Reverse	183 [Sequence]	171	5.8e-92	98.4 [Alignment]

B

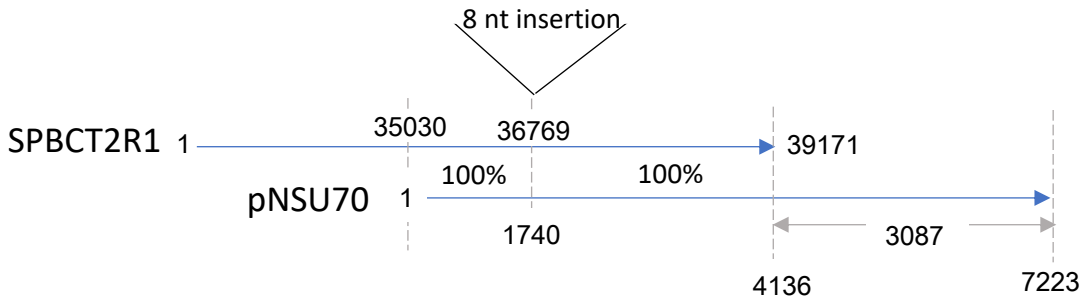

Fig. S2, related to Fig. 1. Construction of a version of the fission yeast genome containing a full-length telomere 2 right. (**A**) Telomeric plasmid pNSU70 (*3*) aligned against the current ASM294v2 version of the *S. pombe* genome using Blast shows a best hit with the right end of chromosome 2. (**B**). Cosmid SPBCT2R1 corresponding to the right end of chromosome 2 (nucleotides 4500619 to 4539800) was aligned with pNSU70 using Clustal Omega (*11*). Nucleotides 4137 to 7223 of pNSU70 were added to chromosome 2 to create a TEL2R-extended version of the genome available under the accession number GSE196149

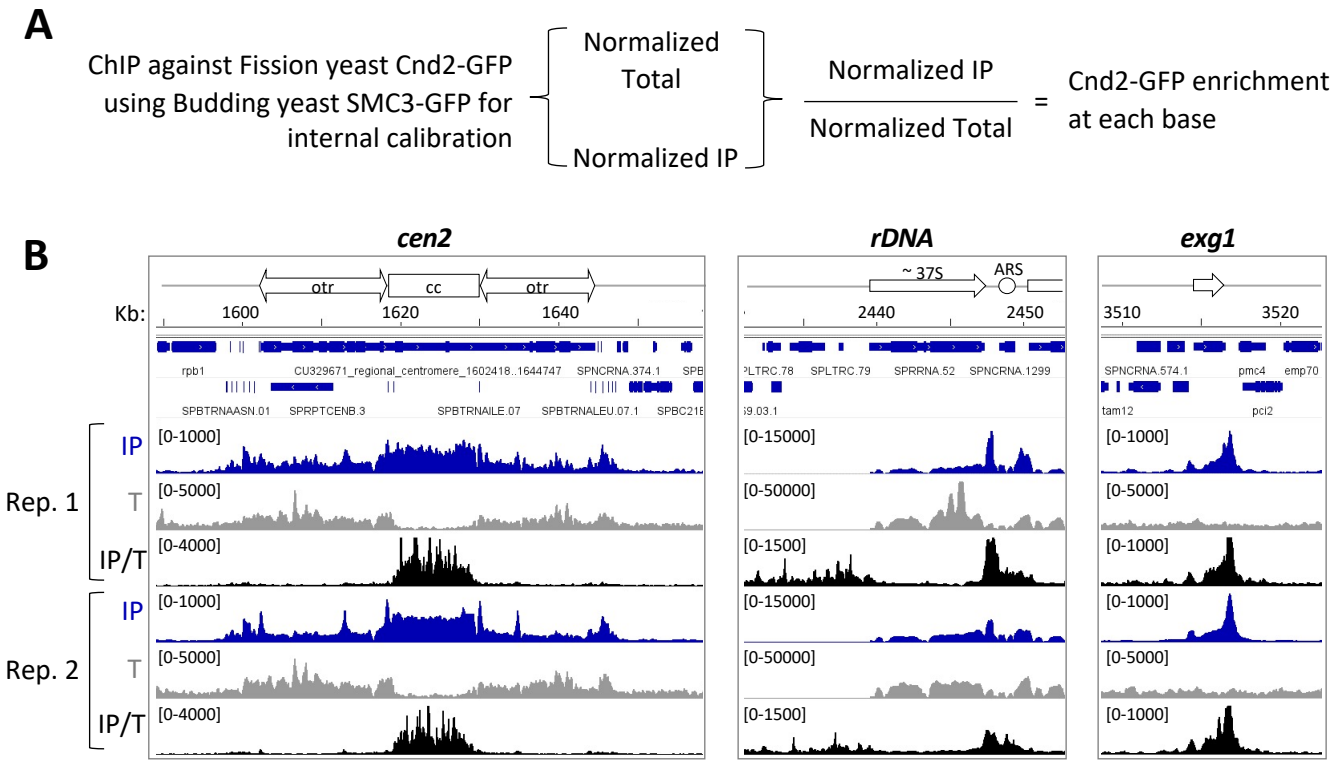

Fig. S3, related to Fig. 1. Base per base ratios of calibrated ChIP-seq signals corrects for biases in coverage. (**A**) Overview of the base per base normalization method applied to correct for biases in coverage in the IP and Total (Input) fractions. (**B**) Calibrated read counts at centromere 2 (*cen 2*), composed of a central core (cc) flanked by repetitive heterochromatic outer repeats (otr) and at rDNA repeats. The single-copy gene *exg1* serves as a non-repetitive control. Mappings have been done on the TEL2R-extented-ASM294v2 version of fission genome. Shown are the results of two biological and technical replicates (Rep.).

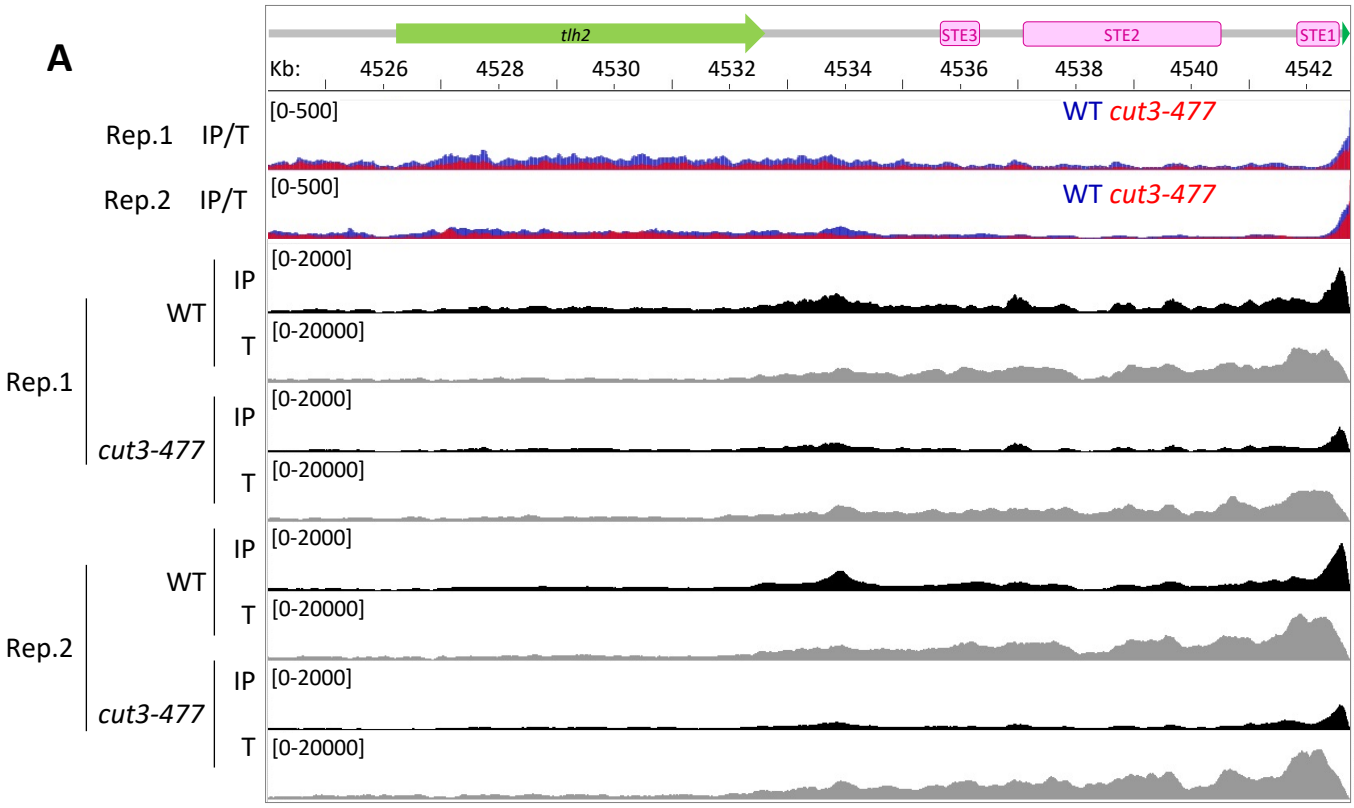

Calibrated ChIP-seq of cnd2-GFP from metaphase arrested cells. First panel shows the ratio between calibrated IP and Inputs (T, total) obtained for two biological and technical replicates (Rep.). Second panel shows the alignments of the corresponding IP and Input samples.

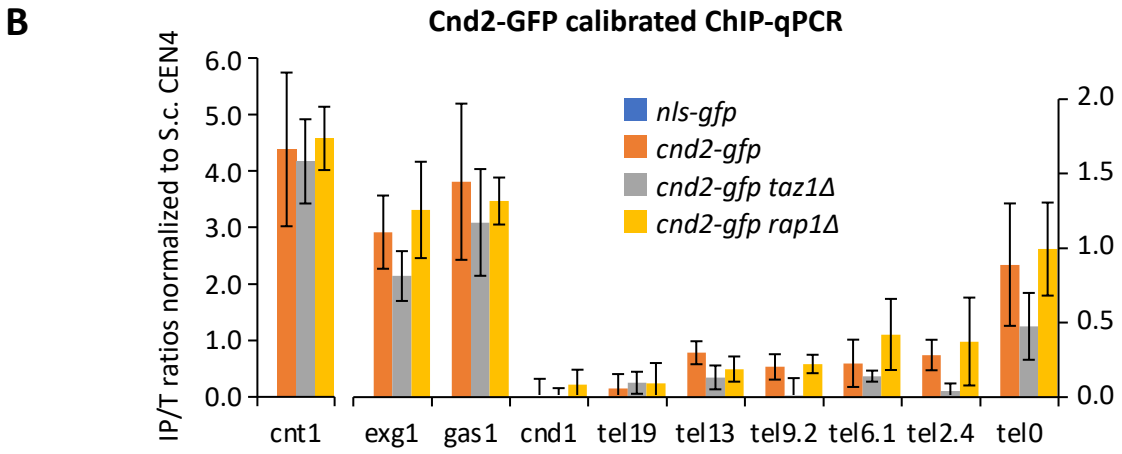

Fig. S4, related to Fig. 1. Condensin is enriched at telomere repeats in a Taz1-dependent manner. (A) Calibrated ChIP-seq read counts from two biological and technical replicates (Rep.). Data from Rep. 1 are also shown in Figure 1. Shown are the normalized read-counts form the ChIP (IP) and Total (T) fractions, and the corresponding base per base IP/T ratios. (**B**) Cnd2-GFP calibrated ChIP-qPCR shown in Figure 1C were normalized with respect to their corresponding IP/T ratios of budding SMC3-GFP at CEN4. *cnt1* is the kinetochore domain of *cen1*, *exg1*, *gas1* and *cnd1* are high or low occupancy binding sites on chromosome arms. Shown are the average and standard deviations from n=3 biological and technical replicates

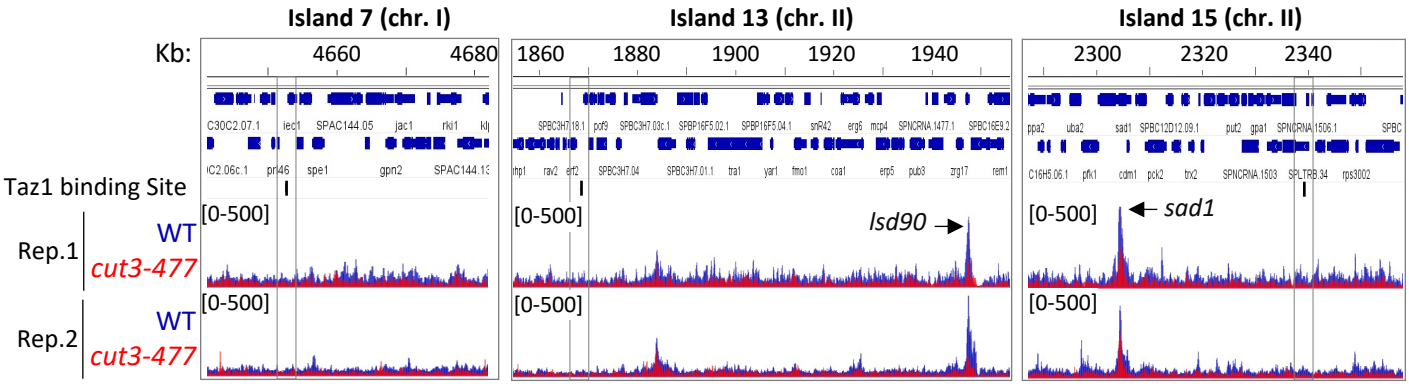

Island	Loci	Taz1 binding	Condensin enrichment
Is3	spac23h3.14	++	-
Is7	spac144.02	++	-
Is13	spbc3h7.08c	+++	-
Is14	eno101	++	-
Is15	spbc26c6.09c	++	-
Is19	spbc1259.02c	+	-

Fig. S4, related to Fig. 1. Condensin is enriched at telomere repeats in a Taz1-dependent manner. (A) Calibrated ChIP-seq read counts from two biological and technical replicates (Rep.). Data from Rep. 1 are also shown in Figure 1. Shown are the normalized read-counts form the ChIP (IP) and Total (T) fractions, and the corresponding base per base IP/T ratios. (**B**) Cnd2-GFP calibrated ChIP-qPCR shown in Figure 1C were normalized with respect to their corresponding IP/T ratios of budding SMC3-GFP at CEN4. *cnt1* is the kinetochore domain of *cen1*, *exg1*, *gas1* and *cnd1* are high or low occupancy binding sites on chromosome arms. Shown are the average and standard deviations from n=3 biological and technical replicates

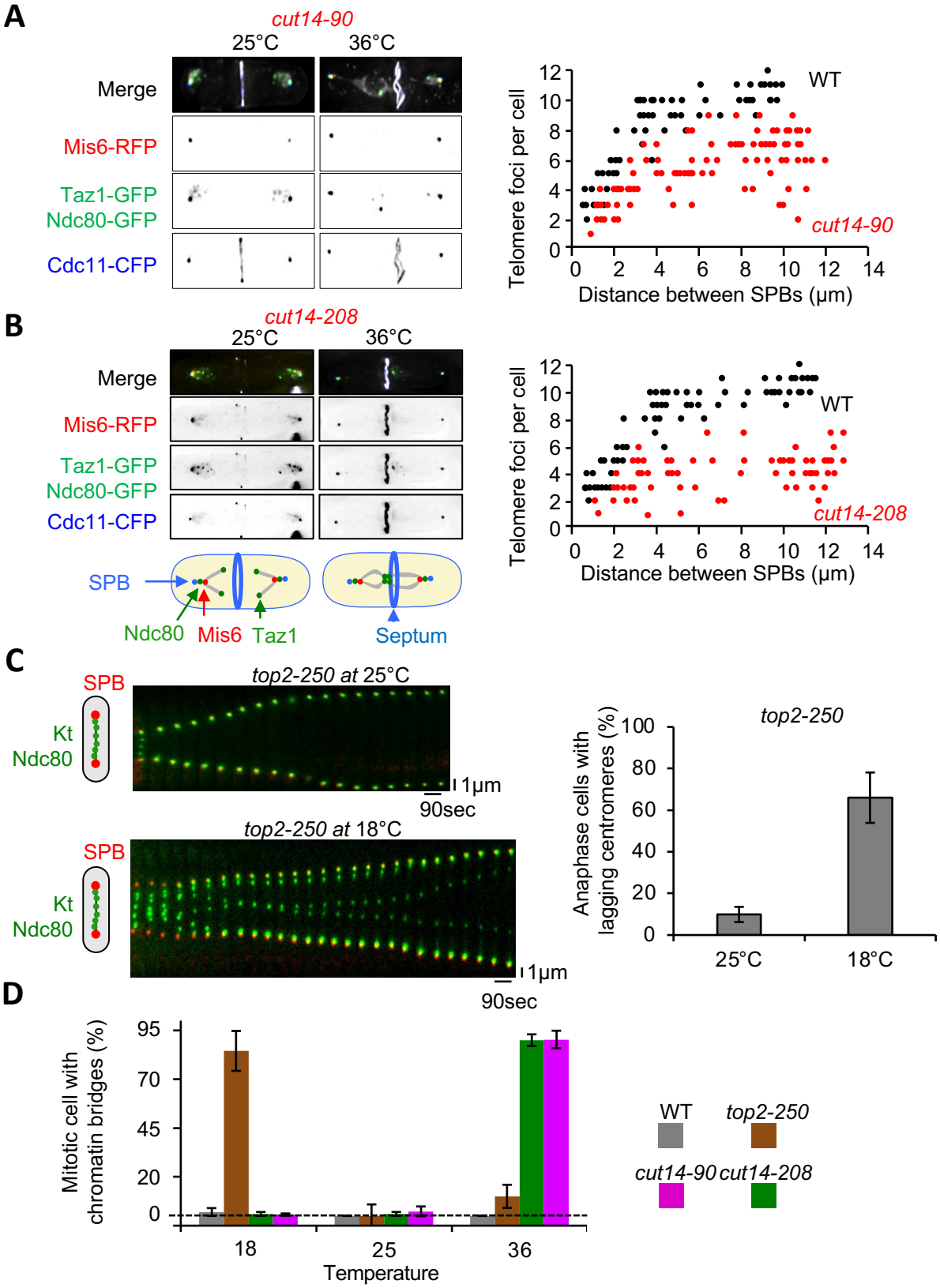

Fig. S6 related to Fig. 2. Condensin activity controls telomere disjunction in a decatenation-independent manner during anaphase. (**A**) *cut14-90* and (**B**) *cut14-208* condensin mutants were grown at the restrictive temperature of 36°C for three hours, fixed with formaldehyde and observed in the presence of DAPI and Calcofluor to stain DNA and the septum, respectively. Telomeres are visualized via Taz1-GFP (green), kinetochores/centromeres via the co-localization of the Ndc80-GFP (green) and Mis6-RFP (red) signals, and SPBs via Cdc11-CFP (blue). Right panels. Number of telomere foci according to the distance between SPBs in condensin mutants at 36°C compared to WT at 36°C. The data shown are from a single representative experiment out of three repeats. For the experiment shown, n>70 cells for each condition. (**C**) Kymograph representation of kinetochore dynamics in live *top2-250* mutant cells at permissive temperature (25°C) or restrictive temperature (18°C). Kinetochores are visualized via Ndc80-GFP (green) and SPBs via Cdc11-CFP (red). Right panel. Quantification of the percentage of *top2-250* anaphase cells showing lagging centromeres. Error bars indicate SD obtained from three independent experiments (n=100 for each condition). (**D**). Percentage of anaphase cells displaying chromatin bridges in wild-type (grey), *top2-250* (brown), *cut14-208* (green), or *cut14-90* (purple) cells grown at the permissive or restrictive temperature for 3 hours. Error bars indicate SD obtained from three independent experiments (n=100 for each condition).

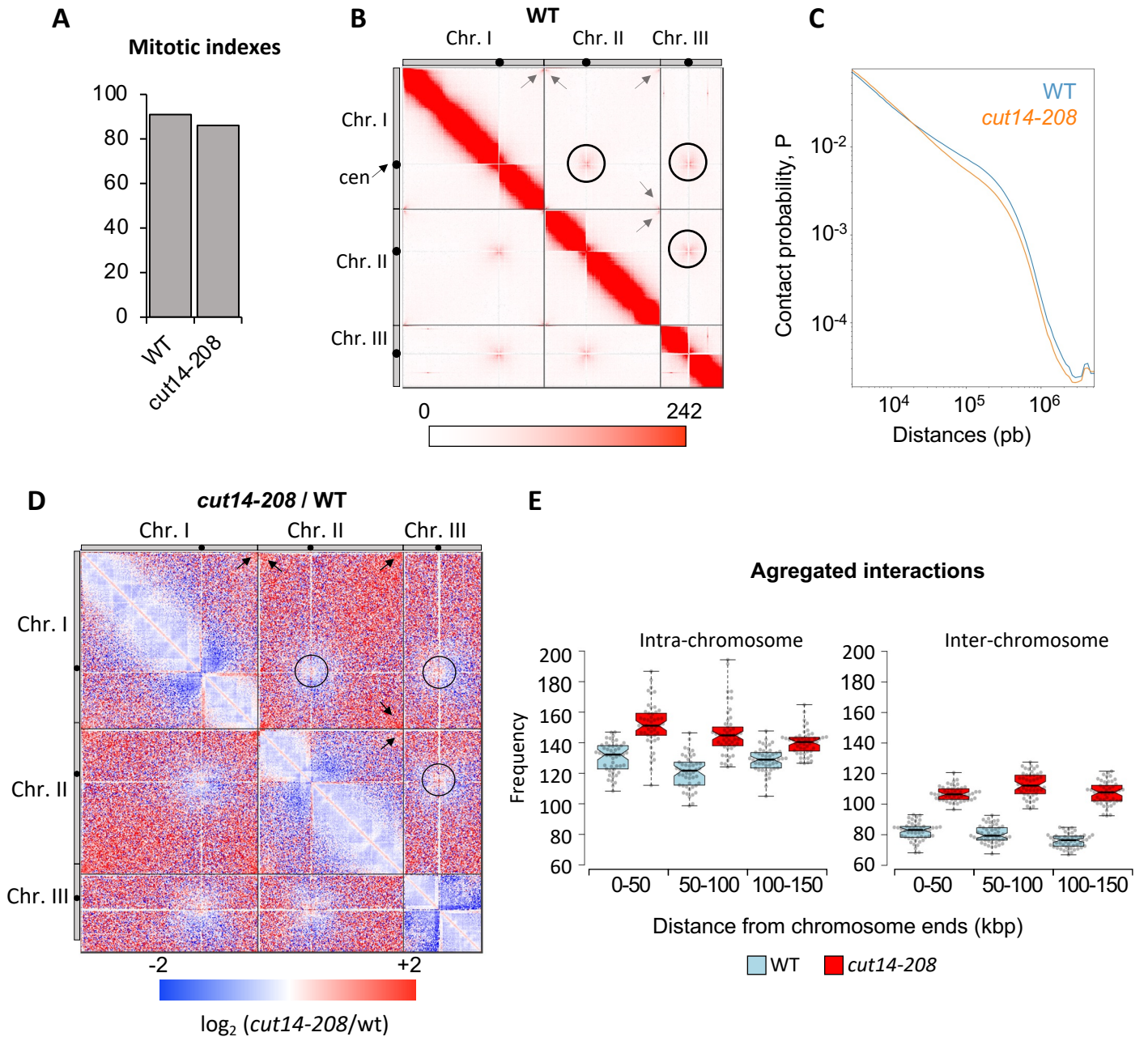

Fig. S7, related to Fig. 3. Condensin deficiency increases contact frequencies between telomeres in metaphase. Data from the biological and technical replicate of those shown Fig. 3. (**A**) Mitotic indexes of cell cultures used for Hi-C. (**B**) Hi-C contact probability matrix at 25 kb resolution of wild-type cells arrested in metaphase at 33°C. Contacts between telomeres (arrows) and centromeres (circles) are indicated (**C**) Median contact probabilities as a function of distance along the chromosomes for wild-type and cut14-208 cells arrested in metaphase at 33°C. (**D**) Hi-C difference map at 25 kb resolution comparing *cut14-208* and wild-type cells. (**E**) Aggregation of contact frequencies at chromosome ends in wild-type and cut14-208 mutant cells in metaphase at 33°C. Boxes indicate the median, 1st and 3rd quartiles, whiskers extend to minimum and maximum values and notches represent the 95% confidence interval for each median. Data points are shown as grey circles.

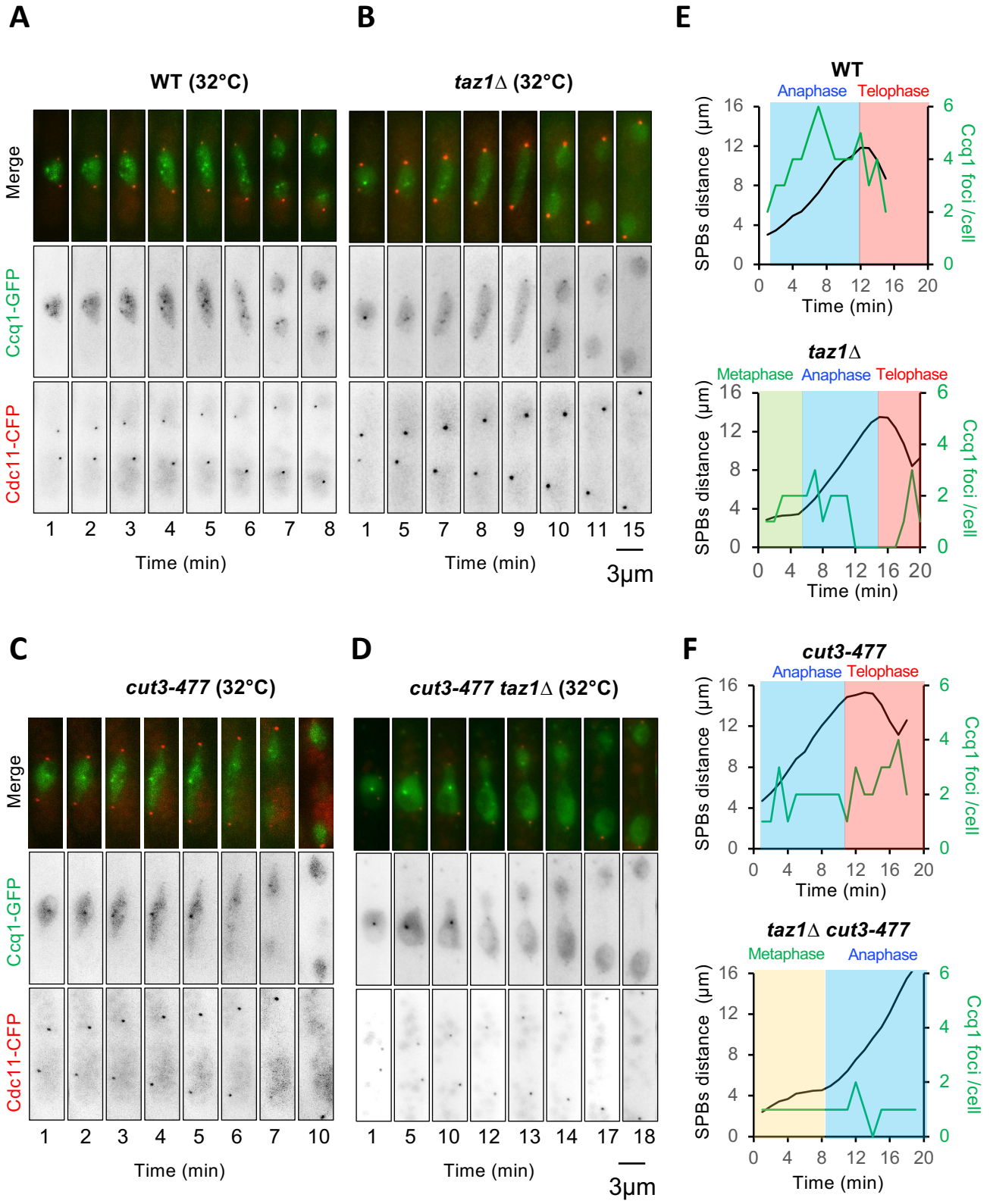

Fig. S8, related to Fig. 4. Taz1 and condensin act in synergy for telomere disjunction in anaphase. (**A-D**) Micrographs from video-microscopy analysis of telomere dissociation in live cells following temperature shift at 32°C for 2 hours: (A) wildtype, (B) *taz1*Δ, (C) *cut3-477*, (D) *cut3-477 taz1*Δ. (**E-F**) Single cell analysis of movies corresponding to A-D, illustrating the number of detectable Ccq1-GFP foci (green curve) according to spindle length (black curve). The data shown are from a single representative movie out of three experimental repeats (n>10 movies for each experiment).

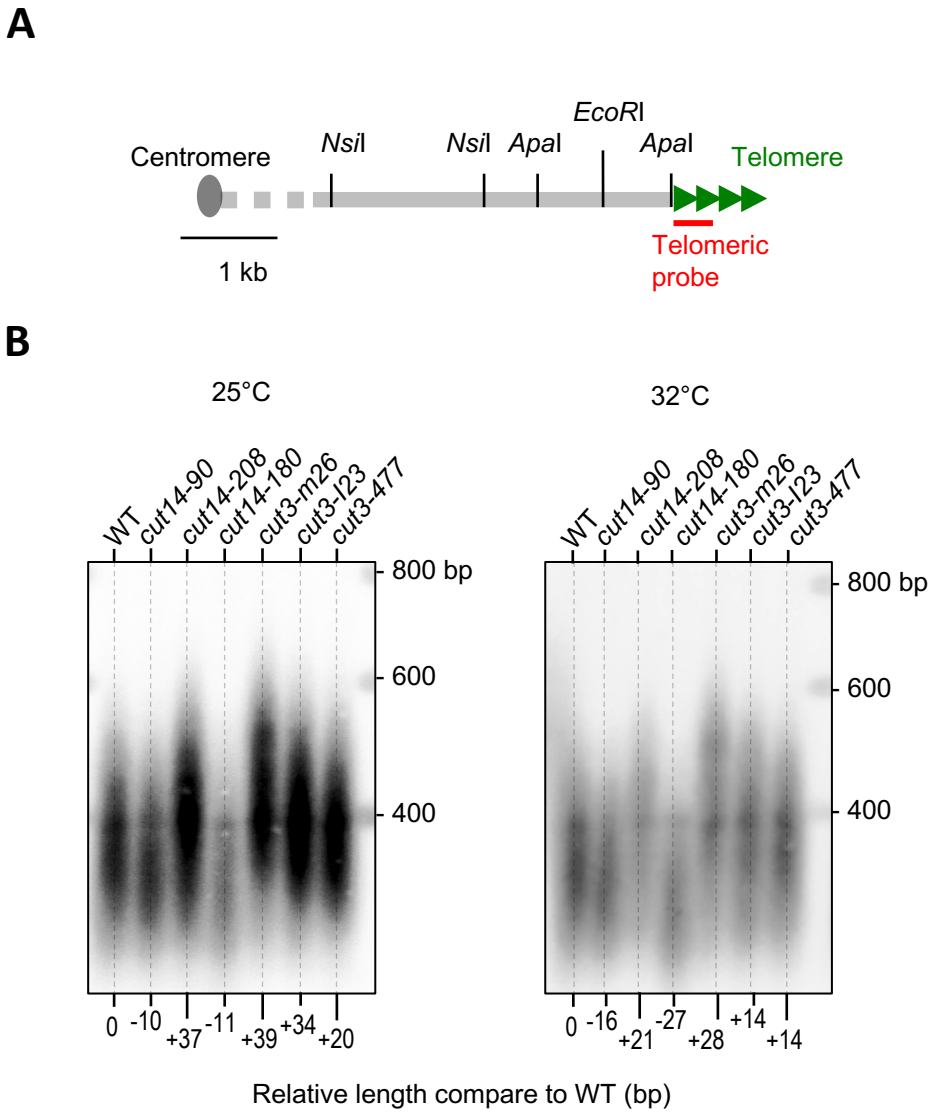

Fig. S9. Mutations in condensin lead to variations in telomere length. (**A**) Relative position of the restriction sites in the telomeric and subtelomeric regions of *S. pombe* chromosomes based on pNSU70 plasmid. The telomeric probe is represented by a red bar. (**B**) Genomic DNA from the indicated strains at the indicated temperatures was digested with *Apa*I and Southern blotted. The membrane was hybridized with the telomeric probe that reveals telomeric signal. The relative gain or loss of telomeric DNA compare to WT is indicated.